Heralded atomic nonadiabatic holonomic quantum computation with Rydberg blockade

Yi-Hao Kang [1,2] Zhi-Cheng Shi,[1,2] Jie Song,[3] and Yan Xia[1,2,*]

[1]*Fujian Key Laboratory of Quantum Information and Quantum Optics (Fuzhou University), Fuzhou 350116, China*
[2]*Department of Physics, Fuzhou University, Fuzhou 350116, China*
[3]*Department of Physics, Harbin Institute of Technology, Harbin 150001, China*

We propose a protocol to realize atomic nonadiabatic holonomic quantum computation (NHQC) with two computational atoms and an auxiliary atom. Dynamics of the system is analyzed in the regime of Rydberg blockade, and robust laser pulses are designed via reverse engineering, so that quantum gates can be easily realized with hig h fidelities. In addition, we also study the evolution suffering from dissipation with a master equation. The result indicates that decays of atoms can be heralded by measuring the state of the auxiliary atom, and nearly perfect unitary evolution can be obtained if the auxiliary atom remains in its Rydberg state. Therefore, the protocol may be helpful to realize NHQC in a dissipative environment.

I. INTRODUCTION

Quantum computation, by means of coherence superpositions of quantum states, has shown many advantages in solving some problems such as factoring and searching [1–4]. To accurately execute quantum computation, high-fidelity quantum gates are essential. However, in the implementations of quantum gates with realistic physical systems, imperfections like systematic errors, classical parameter fluctuation, and dissipation all limit gate fidelities. Therefore, how to eliminate or reduce influence of these imperfections is a critical problem in the realization of practical quantum computation.

In recent years, concepts of nonadiabatic geometric quantum computation (NGQC) [5–10] based on an Abelian geometric phase and nonadiabatic holonomic quantum computation (NHQC) [11–16] based on a non-Abelian geometric phase have been proposed in order to enhance robustness against experimental imperfections. NHQC has shown advantages in various ways. First, as geometric phases are determined by global properties of evolution paths, they are insensitive to classical parameter fluctuation over cyclic evolution [17–24]. Thus, NHQC can be well performed in the presence of classical parameter fluctuation [25,26]. Second, compared with traditional adiabatic holonomic quantum computation (AHQC) [27–30], NHQC releases variations of parameters from limitation of the adiabatic condition, consequently reducing exposure of physical systems to dissipation. Third, recent researches [31–34] have shown that NHQC can be implemented in a flexible way, compatible with many control and optimal methods, e.g., reverse engineering [35–43] and the systematic-error optimal method [44–47]. Therefore, robustness of NHQC against systematic errors can be greatly improved by combining with proper techniques. To date, taking advantage of NHQC, many robust protocols for quantum computation [48–55] have been put forward. Moreover, stability of NHQC has also been demonstrated in a number of experiments [56–61].

In the implementation of NHQC, the time required is shortened compared with AHQC, and quantum information can be encoded in decoherence-free subspace. However, lossy intermediate states, such as excited states of atoms and states of nonvacuum cavity, may still be required as auxiliaries [62–66]. During operations, dissipation acting on these intermediate states, such as energy relaxation and cavity photon leakage, also spoils the unitary evolution. As a result, a system initially in a pure state would finally be in a mixed state after operations, and fidelities of NHQC decrease simultaneously. To further improve fidelities of NHQC for constructions of functional quantum computers, more efforts should be made to diminish the impact of dissipation. Fortunately, researches in the past few years have shown some interesting ways to overcome the influence of dissipation in quantum evolutions. Especially, one approach suggests to design physical systems in order that decays of qubits can be reported by measuring auxiliary qubits, which have been successfully used in protocols [67–70] for generating pure entangled states, namely heralded entanglement generation. More interestingly, the heralded protocols can even be extended to the implementations of quantum gates [71,72], where perfect unitary evolutions can be maintained in a dissipative environment if correct results are reported in measurements of auxiliary qubits. The inspiring ideas of the heralded protocols prompt us to ask whether they can be incorporated in NHQC, so that quantum computation can be implemented with comprehensive resistance to systematic errors, classical parameter fluctuation, and dissipation.

In this paper, we present a protocol to realize heralded NHQC with a physical system containing two computational atoms and an auxiliary atom. With the help of Rydberg blockade, we restrict the evolution in a twelve-dimensional subspace. Afterwards, the evolution is further studied by

*xia-208@163.com

invariant-based reverse engineering, where paths for NHQC are naturally constructed by eigenvectors of an invariant. Moreover, the parameters are meticulously selected by nullifying systematic error sensitivity. Numerical results demonstrate that the implementations of quantum gates are insensitive to systematic errors of laser pulses. Furthermore, dissipation is also taken into account. By analyzing the evolution governed by a master equation, we show that decays of atoms can be reported by measuring the state of the auxiliary atom after operations, and the unitary operation can be maintained if the auxiliary atom is still in its Rydberg state. Compared with the previous Rydberg-atom-based NHQC protocol [64], in which the system may become in a mixed state in the presence of dissipation, the system in the current protocol can remain in a pure state with correct measurement result. Last but not least, the protocol also benefits a lot from the merits of Rydberg atoms and Rydberg blockade. For example, the long lifetime of Rydberg states [73–75] is helpful to produce high success probability of the protocol. Moreover, Rydberg blockade is also a great help to reduce mechanical effects and ionization [76–79] which play significant roles when multiple atoms are excited to their Rydberg states. Overall, the protocol shares advantages of geometric phase, reverse engineering, systematic-error-sensitivity nullified optimal control, heralded implementation, and stability of Rydberg states. Therefore, the protocol may provide useful perspectives in the realization of high-fidelity quantum computation.

The article is organized as follows. In Sec. II, we review the theories for realizing NHQC with invariant-based reverse engineering. In Sec. III, we give the effective Hamiltonian of an atomic system and study the evolution under the influence of dissipation. In Sec. IV, we amply discuss implementations of arbitrary single-qubit gates with invariant-based reverse engineering, and select robust parameters by nullifying the systematic error sensitivity. In Sec. V, we describe the invariant-based implementations of two-qubit entangling gates. In Sec. VI, we perform numerical simulations to check the performance of the implementations of single- and two-qubit gates. Finally, conclusions are given in Sec. VII.

II. THEORETICAL PREPARATION

A. Lewis-Riesenfeld invariant theory

Let us first briefly review the Lewis-Riesenfeld invariant theory [80]. We assume that a Hermitian operator $I(t)$ obeys the equation ($\hbar = 1$)

$$i\frac{\partial}{\partial t}I(t) - [H(t), I(t)] = 0, \quad (1)$$

with $H(t)$ being the Hamiltonian of the considered physical system. If $|\phi_l(t)\rangle$ is a nondegenerate eigenvector of $I(t)$, one can derive a solution of the time-dependent Schrödinger equation $i|\dot{\psi}(t)\rangle = H(t)|\psi(t)\rangle$ as $|\psi_l(t)\rangle = \exp[i\alpha_l(t)]|\phi_l(t)\rangle$, where $\alpha_l(t)$ is the Lewis-Riesenfeld phase for $|\phi_l(t)\rangle$ defined as

$$\alpha_l(t) = \int_0^t \langle\phi_l(t')|i\frac{\partial}{\partial t'} - H(t')|\phi_l(t')\rangle dt'. \quad (2)$$

Therefore, the dynamic invariant $I(t)$ can help us to analyze the evolution of the system. In practice, a very useful way to

construct a dynamic invariant is to use Lie algebra [81,82]. After constructing a dynamic invariant $I(t)$, by making a proper ansatz for parameters of $I(t)$, one can reversely derive Hamiltonian $H(t)$ via Eq. (1) [83]. We will make some introductions about Lie-algebra-based construction of invariants and reverse engineering of the Hamiltonian in Sec. II B.

B. Construction of invariants and reverse engineering of Hamiltonian by using Lie algebra

We consider a system with Hamiltonian $H(t)$, which can be expressed by Hermitian generators $\{G_m | m = 1, 2, \ldots, \tilde{m}\}$ [satisfying the orthogonal condition with the Hilbert-Schmidt inner product $(G_m, G'_m) = \text{Tr}(G_m G_{m'}^\dagger) = 0, m \neq m'$] of a Lie algebra $\mathcal{G}$ (dynamical algebra [84]) as $H(t) = \sum_{m=1}^{\tilde{m}} h_m(t)G_m$ with $\{h_m(t)\}$ being real parameters. In addition, we assume an invariant $I(t)$ in the form of $I(t) = \sum_{m=1}^{\tilde{m}} \xi_m(t)G_m$ with $\{\xi_m(t)\}$ being real parameters. Thus, both $H(t)$ and $I(t)$ can be deemed vectors in $\mathcal{G}$ with basis $\{G_m\}$. Defining a linear transformation $\mathscr{F}_m : \mathcal{G} \mapsto \mathcal{G}$ related to G_m and acting on arbitrary vector $X \in \mathcal{G}$ as $\mathscr{F}_m X = -i[G_m, X]$, we can construct linear transformations $\mathcal{G} \mapsto \mathcal{G}$ related to the Hamiltonian $H(t)$ and the invariant $I(t)$ as $\mathscr{H}(t) = \sum_{m=1}^{\tilde{m}} h_m(t)\mathscr{F}_m$ and $\mathscr{I}(t) = \sum_{m=1}^{\tilde{m}} \xi_m(t)\mathscr{F}_m$, respectively. Thus, Eq. (1) can be rewritten by $\dot{I}(t) = \mathscr{H}(t)I(t)$, which is a set of first-order linear differential equations. According to the existence theorem of solutions for first-order linear differential equations [85], one can find a solution for $I(t)$ theoretically. Therefore, the assumption $I(t) = \sum_{m=1}^{\tilde{m}} \xi_m(t)G_m$ is proper.

Although one can always find an invariant in the dynamical algebra with given Hamiltonian parameters $\{h_m(t)\}$ in theory, the process of obtaining analytical solution of $I(t)$ with $\dot{I}(t) = \mathscr{H}(t)I(t)$ is usually very complex. Thus, instead of solving the invariant $I(t)$ with known $\{h_m(t)\}$, reverse engineering suggests to reversely derive the Hamiltonian of the system by using parameters $\{\xi_m(t)\}$. For this purpose, we rewrite Eq. (1) as $\dot{I}(t) = \mathscr{I}(t)H(t)$. Since $\mathscr{I}(t)I(t) = 0$, $\mathscr{I}(t)$ is a singular matrix, consequently $\mathscr{I}^{-1}(t)$ does not exist. Thus, $H(t)$ cannot be solved by $H(t) = \mathscr{I}^{-1}(t)I(t)$. In practice, one can apply Gauss elimination or pseudoinverse matrices [82] to solve $H(t)$. Here, we take Gauss elimination as an example to illustrate the process of reverse engineering. Noticing that some of controls in $\{G_m\}$ may be unavailable in some specific systems, we first partition $\mathscr{I}(t)$ and $H(t)$ as

$$\mathscr{I}(t) = \begin{bmatrix} \mathscr{I}^{(1)}_{\tilde{m}\times\tilde{m}_1}(t) & \mathscr{I}^{(2)}_{\tilde{m}\times\tilde{m}_2}(t) \end{bmatrix}, \quad H(t) = \begin{bmatrix} H_{\tilde{m}_1}(t) \\ O_{\tilde{m}_2}(t) \end{bmatrix}, \quad (3)$$

with $\tilde{m}_1$ and $\tilde{m}_2$ being numbers of available and unavailable controls, respectively. In this case, we obtain equation as $\mathscr{I}^{(1)}_{\tilde{m}\times\tilde{m}_1}(t)H_{\tilde{m}_1}(t) = \dot{I}$. We assume that the rank of $\mathscr{I}^{(1)}_{\tilde{m}\times\tilde{m}_1}(t)$ is $\tilde{m}_3$ ($\tilde{m}_3 \leqslant \tilde{m}_1$ is always satisfied due to the property of rank). Thus, one can transform $\mathscr{I}^{(1)}_{\tilde{m}\times\tilde{m}_1}(t)$ to

$$\tilde{\mathscr{I}}^{(1)}_{\tilde{m}\times\tilde{m}_1}(t) = \mathscr{R}(t)\mathscr{I}^{(1)}_{\tilde{m}\times\tilde{m}_1}(t) = \begin{bmatrix} \tilde{\mathscr{I}}^{(1)}_{\tilde{m}_3\times\tilde{m}_1}(t) \\ O_{\tilde{m}_4\times\tilde{m}_1}(t) \end{bmatrix} \quad (4)$$

by a set of elementary row transformations as $\mathscr{R}(t)$ with $\tilde{m}_4 = \tilde{m} - \tilde{m}_3$. Then, we can partition $\dot{\tilde{I}}(t) = \mathscr{R}(t)\dot{I}(t)$ as $\dot{\tilde{I}}(t) = [\dot{\tilde{I}}_{\tilde{m}_3}(t) \ \dot{\tilde{I}}_{\tilde{m}_4}(t)]^T$, and derive $\tilde{\mathscr{I}}^{(1)}_{\tilde{m}_3\times\tilde{m}_1}(t)H_{\tilde{m}_1}(t) = \dot{\tilde{I}}_{\tilde{m}_3}(t)$ and $\dot{\tilde{I}}_{\tilde{m}_4}(t) = 0$. $\dot{\tilde{I}}_{\tilde{m}_4}(t) = 0$ is a set of constraint equations for

parameters $\{\xi_m(t)\}$. Thus, the number of independent parameters in $\{\xi_m(t)\}$ is $\tilde{m}_3$. In addition, because of $\tilde{m}_3 \leqslant \tilde{m}_1$, solutions of equation $\tilde{\mathcal{I}}^{(1)}_{\tilde{m}_3 \times \tilde{m}_1}(t) H_{\tilde{m}_1}(t) = \dot{\tilde{I}}_{\tilde{m}_3}(t)$ always exist. When $\tilde{m}_1 = \tilde{m}_3$, $H_{\tilde{m}_1}(t)$ have a unique solution $[\tilde{\mathcal{I}}^{(1)}_{\tilde{m}_3 \times \tilde{m}_1}(t)]^{-1} \dot{\tilde{I}}_{\tilde{m}_3}(t)$. When $\tilde{m}_1 > \tilde{m}_3$, one can obtain multiple solutions of $H_{\tilde{m}_1}(t)$, and the number of linearly independent solutions is $(\tilde{m}_1 - \tilde{m}_3)$.

C. Nonadiabatic holonomic quantum computation with eigenvectors of dynamic invariant

To realize nonadiabatic holonomic quantum computation (NHQC) in a computational subspace $\mathcal{S}$, an alternative way is to select a set of time-dependent vectors $\{|\tilde{\psi}_l(t)\rangle\}$ spanning $\mathcal{S}$ and meeting the cyclic evolution condition $|\tilde{\psi}_l(0)\rangle = |\tilde{\psi}_l(T)\rangle$ (T is the total operation time). According to Ref. [31], if the operator $\tilde{\Xi}_l(t) = |\tilde{\psi}_l(t)\rangle\langle\tilde{\psi}_l(t)|$ obeys the von Neumann equation

$$\frac{d}{dt}\tilde{\Xi}_l(t) = -i[H(t), \tilde{\Xi}_l(t)], \qquad (5)$$

the evolution in subspace $\mathcal{S}$ can be described as

$$U(T, 0) = \sum_l e^{i[\tilde{\vartheta}_l(T) + \tilde{\Theta}_l(T)]} \tilde{\Xi}(0), \qquad (6)$$

with

$$\tilde{\vartheta}_l(t) = -\int_0^t \langle\tilde{\psi}_l(t')|H(t')|\tilde{\psi}_l(t')\rangle dt' \qquad (7)$$

and

$$\tilde{\Theta}_l(t) = \int_0^t \langle\tilde{\psi}_l(t')|i\frac{\partial}{\partial t'}|\tilde{\psi}_l(t')\rangle dt' \qquad (8)$$

being the dynamic phase and the geometric phase acquired by $|\tilde{\psi}_l(t)\rangle$ during the time interval $[0, T]$. Therefore, the evolution becomes purely geometric when $\vartheta_l(T) = 0$ for all vectors in $\{|\tilde{\psi}_l(t)\rangle\}$. In practice, eigenvectors of a dynamic invariant constitute an alternative candidate to construct vectors $\{|\tilde{\psi}_l(t)\rangle\}$. According to Ref. [33], for a nondegenerate eigenvector $|\phi_l(t)\rangle$ of a dynamic invariant, the von Neumann equation

$$\frac{d}{dt}\Xi_l(t) = -i[H(t), \Xi_l(t)], \qquad (9)$$

with $\Xi_l(t) = |\phi_l(t)\rangle\langle\phi_l(t)|$ being naturally satisfied. Therefore, if a set of nondegenerate eigenvectors $\{|\phi_l(t)\rangle\}$ of a dynamic invariant span the computational subspace $\mathcal{S}$, the condition to realize NHQC is to eliminate the dynamic part of the Lewis-Riesenfeld phase acquired in $[0, T]$ as

$$\vartheta_l(T) = -\int_0^T \langle\phi_l(t)|H(t)|\phi_l(t)\rangle dt = 0. \qquad (10)$$

Accordingly, the remaining part of Lewis-Riesenfeld phase,

$$\Theta_l(T) = \int_0^t \langle\phi_l(t)|i\frac{\partial}{\partial t}|\phi_l(t)\rangle dt, \qquad (11)$$

is purely geometric.

III. DYNAMICS OF THE ATOMIC SYSTEM IN THE RYDBERG BLOCKADE REGIME

A. Physical model and Hamiltonian

We consider a system containing three atoms 0, 1, and 2 whose level configurations are shown in Fig. 1. The atom 0 has a ground level $|0\rangle_0$ and a Rydberg state $|r\rangle_0$, and is used as an auxiliary qubit. The transition $|0\rangle_0 \leftrightarrow |r\rangle_0$ is driven by two pairs of laser pulses. One pair possesses Rabi frequencies $\Omega_{01}(t)$ and $\Omega'_{01}(t)$ with different detunings $\pm\Delta_1$, respectively [positive (negative) corresponding to blue (red) detuning] [86]. The other pair possesses Rabi frequencies $\Omega_{02}(t)$ and $\Omega'_{02}(t)$ with different detunings $\pm\Delta_2$, respectively. Besides, the atom k ($k = 1, 2$) is employed as a computational atom, possessing two ground levels $|0\rangle_k$ and $|1\rangle_k$ as computational basis and a Rydberg state $|r\rangle_k$ as an auxiliary level. The transition $|j - 1\rangle_k \leftrightarrow |r\rangle_k$ ($j = 1, 2$) is driven by two pairs of laser pulses, one pair with Rabi frequencies $\Omega_{kj}(t)$ and $\Omega'_{kj}(t)$ and different detunings $\pm\Delta_k$, the other pair with Rabi frequencies $\Omega_{kj3}(t)$ and $\Omega'_{kj3}(t)$ and different detunings $\pm\Delta_3$. We assume that, between each two atoms, there exists a Rydberg interaction with strength V [87].

To parametrize the Rabi frequencies for the implementation of the NHQC, we set

$$\Omega_{k0} = \Omega_k(t)\cos(\theta_k/2), \quad \Omega'_{k0} = \Omega'_k(t)\cos(\theta_k/2),$$

$$\Omega_{k1} = \Omega_k(t)\sin(\theta_k/2)e^{i\varphi_k}, \quad \Omega'_{k1} = \Omega'_k(t)\sin(\theta_k/2)e^{i\varphi_k},$$

$$\Omega_{k03} = \Omega_{k3}(t)\cos(\theta_k/2), \quad \Omega'_{k03} = \Omega'_{k3}(t)\cos(\theta_k/2),$$

$$\Omega_{k13} = \Omega_{k3}(t)\sin(\theta_k/2)e^{i\varphi_k}, \quad \Omega'_{k13} = \Omega'_{k3}(t)\sin(\theta_k/2)e^{i\varphi_k}, \qquad (12)$$

with θ_k and φ_k being two time-independent parameters. In addition, we assume

$$\Omega_k(t) = e^{i\mu_k(t)}\bar{\Omega}_k(t), \quad \Omega'_k(t) = e^{i\mu'_k(t)}\bar{\Omega}_k(t),$$

$$\Omega_{0k}(t) = \Omega'_{0k}(t) = -\bar{\Omega}_{0k}(t), \quad \Omega_{13}(t) = e^{i\mu_3(t)}\bar{\Omega}_{k3}(t),$$

$$\Omega'_{13}(t) = e^{i\mu'_3(t)}\bar{\Omega}_{k3}(t), \quad \Omega_{23}(t) = \Omega'_{23}(t) = -\bar{\Omega}_{23}(t), \qquad (13)$$

with $\{\bar{\Omega}_k(t), \bar{\Omega}_{0k}(t), \bar{\Omega}_{k3}(t)\}$ being real functions. In the regime of Rydberg blockade, the effective Hamiltonian of the system can be derived as (detailed derivations are shown in Appendix A)

$$H_e(t) = H_{e_0}(t) + H_{e_1}(t) + H_{e_2}(t) + H_{e_3}(t),$$

$$H_{e_0}(t) = \tilde{\Omega}_1(t)e^{i\mu_1(t)}|r + +\rangle_{012}\langle 0r + |$$
$$\qquad + \tilde{\Omega}_2(t)e^{i\mu_2(t)}|r + +\rangle_{012}\langle 0 + r| + \text{H.c.}$$

$$H_{e_1}(t) = \tilde{\Omega}_1(t)e^{i\mu_1(t)}|r + -\rangle_{012}\langle 0r - | + \text{H.c.},$$

$$H_{e_2}(t) = \tilde{\Omega}_2(t)e^{i\mu_2(t)}|r - +\rangle_{012}\langle 0 - r| + \text{H.c.},$$

$$H_{e_3}(t) = \tilde{\Omega}_3(t)e^{i\mu_3(t)}|0r+\rangle_{012}\langle 0 + r| + \text{H.c.}, \qquad (14)$$

with

$$\tilde{\Omega}_k(t) = \frac{2\bar{\Omega}_k(t)\bar{\Omega}_{0k}(t)}{\Delta_k}, \quad \tilde{\Omega}_3(t) = \frac{2\bar{\Omega}_{13}(t)\bar{\Omega}_{23}(t)}{\Delta_3},$$

$$|+\rangle_k = \cos(\theta_k/2)|0\rangle_k + \sin(\theta_k/2)e^{i\varphi_k}|1\rangle_k,$$

$$|-\rangle_k = \sin(\theta_k/2)|0\rangle_k - \cos(\theta_k/2)e^{i\varphi_k}|1\rangle_k. \qquad (15)$$
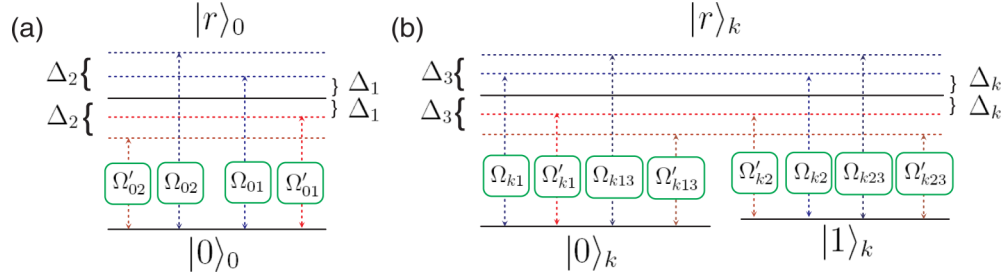
FIG. 1. (a) Level configuration of the auxiliary atom 0. (b) Level configuration of the computational atom k ($k = 1, 2$).

According to Eq. (14), when the auxiliary atom is initially prepared in Rydberg state $|r\rangle_0$, and the computational atoms are in arbitrary states in superposition of computational basis $|\pm\rangle_k$, the evolution is restricted in an eight-dimensional subspace $\mathcal{B} = \text{span}\{|r \pm \pm\rangle_{012}, |0r\pm\rangle_{012}, |0 \pm r\rangle_{012}\}$, which is shown by the levels with blue-dotted lines in Fig. 2.

B. Evolution of the system in a dissipative environment

We now take dissipation into account, and analyze the evolution of the system under the influence of dissipation. For computational atom k, there exist two dissipative paths as $|r\rangle_k \rightarrow |0\rangle_k$ and $|r\rangle_k \rightarrow |1\rangle_k$. Considering the same decay rate $\gamma/2$ for each path, the dissipation of atom k can be described by two Lindblad operators as $L_{\pm k} = \sqrt{\gamma/2}|(1 \pm 1)/2\rangle_k\langle r|$. For the auxiliary atom 0, there exists a dissipative path $|r\rangle_0 \rightarrow |0\rangle_0$. Assuming the decay rate of $|r\rangle_0 \rightarrow |0\rangle_0$ is γ, dissipation of the atom can be described by the Lindblad operator $L_0 = \sqrt{\gamma}|0\rangle_0\langle r|$. The evolution of the total system under the influence of dissipation is governed by the master equation

$$\dot{\rho}(t) = -i[H_e(t), \rho(t)] + \sum_{\iota=-2}^{2} \left[L_\iota \rho(t) L_\iota^\dagger - \frac{1}{2} L_\iota^\dagger L_\iota \rho(t) \right.$$

$$\left. - \frac{1}{2} \rho(t) L_\iota^\dagger L_\iota \right], \tag{16}$$

with $\rho(t)$ being the density operator of the system. When dissipation is taken into account, the evolution of the system no longer remains in the eight-dimensional subspace $\mathcal{B}$, but is confined to a twelve-dimensional subspace $\mathcal{B}' = \text{span}\{|r \pm \pm\rangle_{012}, |0r\pm\rangle_{012}, |0 \pm r\rangle_{012}, |0 \pm \pm\rangle_{012}\}$, which is shown by the

levels with both blue-dotted and red-solid lines in Fig. 2. The nonzero matrix elements of $\dot{\rho}(t)$ is shown in Appendix B, where the results indicate that the density operator can be written as

$$\rho(t) = e^{-\gamma t} U_e(t) \rho(0) U_e^\dagger(t) \oplus \rho'(t), \tag{17}$$

with $U_e(t)$ being the evolution operator given by the equation $i\dot{U}_e(t) = H_e(t)U_e(t)$, and $\rho'(t)$ being part of the density operator shown in Appendix B. We assume that the target operation is $U_e^{\text{ideal}}(T) = |r\rangle_0\langle r| \otimes U_{12} + |0\rangle_0\langle 0| \otimes \mathbb{1}_{12}$ ($\mathbb{1}_{12}$ denotes the identity operation for atoms 1 and 2). Then, $U_e(T)\rho(0)U_e^\dagger(T)$ in the ideal case should be $|r\rangle_0\langle r| \otimes U_{12}\rho_{12}(0)U_{12}^\dagger$, as the auxiliary atom is initially prepared in the Rydberg state. On the other hand, we can also see in Appendix B that all nonzero elements of $\rho'(t)$ do not contain the $|r\rangle_0$ component. Therefore, if one measures the state of the auxiliary atom at $t = T$ and obtains the result $|r\rangle_0$, we confirm that decays of atoms have not happened, and the unitary operation U_{12} on computational atoms 1 and 2 is successfully implemented. According to Eq. (17), the success probability is $P_s = e^{-\gamma T}$. If we consider the decay rate as $\gamma = 1$ kHz [88,89], the success probability is higher than 99% when $T \leqslant 10.1$ μs, and is still higher than 90% when $T \leqslant 105.4$ μs, theoretically.

IV. ARBITRARY SINGLE-QUBIT GATES

A. Construction of the evolution path with invariant-based reverse engineering

In this section, let us first consider the implementation of arbitrary single-qubit gates by using the computational atom 1 and the auxiliary atom 0 with invariant-based reverse engineering. In this case, laser pulses $\Omega_2(t)$, $\Omega_2'(t)$, $\Omega_{02}(t)$,
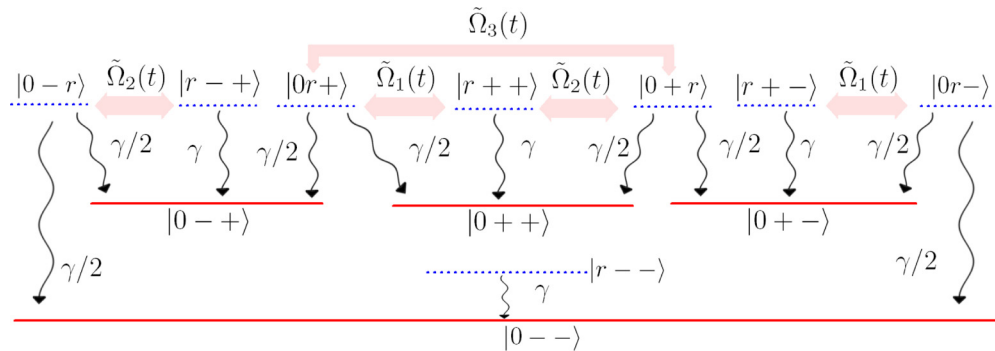

FIG. 2. The subspaces of unitary evolution (levels with blue-dotted lines) and dissipative evolution (levels with blue dotted and red solid lines).

$\Omega'_{02}(t)$, $\Omega_{k3}(t)$, and $\Omega'_{k3}(t)$ are switched off. According to the effective Hamiltonian in Eq. (14), the Hamiltonian for the implementation of singlet-qubit gates read

$$H_s(t) = \tilde{\Omega}_1(t)e^{i\mu_1(t)}|r+\rangle_{01}\langle 0r| + \text{H.c.}$$
$$= \tilde{\Omega}_1(t)\cos[\mu_1(t)]\sigma_x + \tilde{\Omega}_1(t)\sin[\mu_1(t)]\sigma_y + 0 \times \sigma_z, \tag{18}$$

with

$$\sigma_x = |0r\rangle_{01}\langle r+| + \text{H.c.}, \quad \sigma_y = -i|0r\rangle_{01}\langle r+| + \text{H.c.}, \quad \sigma_z$$
$$= |0r\rangle_{01}\langle 0r| - |r+\rangle_{01}\langle r+|, \tag{19}$$

which can be considered as generators of su(2) Lie algebra satisfying commutation relations

$$[\sigma_x, \sigma_y] = 2i\sigma_z, \quad [\sigma_y, \sigma_z] = 2i\sigma_x, \quad [\sigma_z, \sigma_x] = 2i\sigma_y. \tag{20}$$

To find a dynamic invariant with Lie algebra, we consider a dynamic invariant in a superposition of all generators of su(2) algebra as [82]

$$I_s(t) = \lambda_x(t)\sigma_x + \lambda_y(t)\sigma_y + \lambda_z(t)\sigma_z. \tag{21}$$

By substituting Eq. (21) into Eq. (1), we obtain the equations as

$$\dot{\lambda}_x(t) = 2\Omega_y(t)\lambda_z(t), \quad \dot{\lambda}_y(t) = -2\Omega_x(t)\lambda_z(t),$$
$$\dot{\lambda}_z(t) = 2\Omega_x(t)\lambda_y(t) - 2\Omega_y(t)\lambda_x(t), \tag{22}$$

with $\Omega_x(t) = \tilde{\Omega}_1(t)\cos[\mu_1(t)]$ and $\Omega_y(t) = \tilde{\Omega}_1(t)\sin[\mu_1(t)]$. From Eq. (22), we can derive a constraint equation for coefficients of the dynamic invariant $I_s(t)$ as $\lambda_x^2(t) + \lambda_y^2(t) + \lambda_z^2(t) = C^2$ with C being a real constant. Accordingly, for $C = 1$, $\lambda_x(t)$, $\lambda_y(t)$, and $\lambda_z(t)$ can be parametrized as

$$\lambda_x(t) = \sin\beta_1\sin\beta_2, \quad \lambda_y(t) = \sin\beta_1\cos\beta_2,$$
$$\lambda_z(t) = \cos\beta_1, \tag{23}$$

with two time-dependent parameters β_1 and β_2. Using Eqs. (22)–(23), we can reversely solve $\Omega_x(t)$ and $\Omega_y(t)$ as

$$\Omega_x(t) = (\dot{\beta}_2\sin\beta_2\tan\beta_1 - \dot{\beta}_1\cos\beta_2)/2,$$
$$\Omega_y(t) = (\dot{\beta}_2\cos\beta_2\tan\beta_1 + \dot{\beta}_1\sin\beta_2)/2. \tag{24}$$

In addition, eigenvectors of the dynamic invariant $I_s(t)$ can also be obtained as

$$|\phi_+^s(t)\rangle = \cos\frac{\beta_1}{2}|0r\rangle_{01} + ie^{-i\beta_2}\sin\frac{\beta_1}{2}|r+\rangle_{01},$$
$$|\phi_-^s(t)\rangle = ie^{i\beta_2}\sin\frac{\beta_1}{2}|0r\rangle_{01} + \cos\frac{\beta_1}{2}|r+\rangle_{01}, \tag{25}$$

whose eigenvalues are 1 and -1, respectively. By applying the results in Eqs. (10) and (11), the time derivatives of dynamic phases and geometric phases acquired by $|\phi_\pm^s(t)\rangle$ can be respectively calculated by

$$\dot{\vartheta}_\pm(t) = \mp\frac{\dot{\beta}_2\sin^2\beta_1}{2\cos\beta_1}, \qquad \dot{\Theta}_\pm(t) = \pm\dot{\beta}_2\sin^2\frac{\beta_1}{2}. \tag{26}$$

In the implementation of the single-qubit gate, the computational subspace is spanned by $|r\pm\rangle_{01}$. The vector $|r-\rangle_{01}$

is dynamically decoupled to the Hamiltonian $H_s(t)$. Therefore, the evolution with initial state $|r+\rangle_{01}$ is mainly studied here. We consider the boundary condition as $\beta_1(0) = \beta_1(T) = 0$ for cyclic evolution of eigenvectors as $|\phi_\pm^s(0)\rangle = |\phi_\pm^s(T)\rangle$. In this case, the boundary condition of $\beta_2(t)$ is irrelevant to the cyclic evolution condition according to Eq. (25). In addition, the evolution with initial state $|r+\rangle_{01}$ is along the eigenvector $|\phi_-^s(t)\rangle$. In order to eliminate the dynamic phase $\vartheta_-(T)$ and obtain a pure geometric phase $\Theta_-(T) = \Theta_s$, we design parameters $\beta_1(t)$ and $\beta_2(t)$ by dividing the time interval $[0, T]$ into three parts: $[0, \tau_1]$, $[\tau_1, \tau_2]$, and $[\tau_2, T]$. When $t \in [0, \tau_1]$, $\beta_1(t)$ increases from 0 to π, and $\beta_2(t)$ remains an undetermined parameter. When $t \in [\tau_1, \tau_2]$, we keep $\beta_1(t) = \pi$, and let $\beta_2(t) = \beta_2(\tau_1) - \Theta_s(t - \tau_1)/(\tau_2 - \tau_1)$. When $t \in [\tau_2, T]$, we set $\beta_1(t) = \beta_1[\tau_1(T - t)/(T - \tau_2)]$, $\beta_2(t) = -\Theta_s + \beta_2[\tau_1(T - t)/(T - \tau_2)]$, which meet the boundary conditions $\beta_1(\tau_2) = \beta_1(\tau_1) = \pi$, $\beta_1(T) = \beta_1(0) = 0$, $\beta_2(\tau_2) = -\Theta_s + \beta_2(\tau_1)$, and $\beta_2(T) = -\Theta_s$. With the above assumptions of $\beta_1(t)$ and $\beta_2(t)$, the dynamic (geometric) phase acquired in the time interval $[0, \tau_1]$ is nullified by that acquired in time interval $[\tau_2, T]$ (see Appendix C for details). Moreover, in the time interval $[\tau_1, \tau_2]$, as $\beta_1(t)$ is kept at π, the dynamic phase acquired is zero according to Eq. (26). On the other hand, the geometric phase acquired is

$$\Theta_-(\tau_2) - \Theta_-(\tau_1) = -\int_{\tau_1}^{\tau_2}\dot{\beta}_2(t)\sin^2\left[\frac{\beta_1(t)}{2}\right]dt$$
$$= \beta_2(\tau_1) - \beta_2(\tau_2) = \Theta_s. \tag{27}$$

Consequently, the total dynamic phase and the geometric phase acquired in $[0, T]$ are $\vartheta_-(T) = 0$ and $\Theta_-(T) = \Theta_s$. Therefore, the evolution operator can be described as

$$U_s(T, 0) = e^{i\Theta_s}|r+\rangle_{01}\langle r+| + |r-\rangle_{01}\langle r-|$$
$$= e^{i\Theta_s/2}|r\rangle_0\langle r| \otimes e^{i\Theta_s\vec{n}_1\cdot\vec{\sigma}_1/2}, \tag{28}$$

with $\vec{n}_1 = [\sin\theta_1\cos\varphi_1, \sin\theta_1\sin\varphi_1, \cos\theta_1]$, $\vec{\sigma}_1 = [\sigma_{x1}, \sigma_{y1}, \sigma_{z1}]$, $\sigma_{x1} = |0\rangle_1\langle 1| + \text{H.c.}$, $\sigma_{y1} = -i|0\rangle_1\langle 1| + \text{H.c.}$, and $\sigma_{z1} = |0\rangle_1\langle 0| - |1\rangle_1\langle 1|$. Up to a global phase $\Theta_s/2$, Eq. (28) represents a rotation operator around the axis $\vec{n}$ with rotation angle $\Theta_s/2$, which can generate arbitrary single-qubit gates [90,91]. Specially, when $(\Theta_s, \theta_1, \varphi_1) = \pi(1, 1/2, 1)$, we get a NOT gate for atom 1 as $U_N = \sigma_{x1}$; when $\theta_1 = \pi$, we obtain a Θ_s phase gate for atom 1 as $U_{\Theta_s} = \text{diag}[1, \exp(i\Theta_s)]$; when $(\Theta_s, \theta_1, \varphi_1) = \pi(1, -1/4, 0)$, a Hadamard gate $U_H = (\sigma_{x1} + \sigma_{z1})/\sqrt{2}$ for atom 1 is realized.

The design of parameters $\beta_1(t)$ and $\beta_2(t)$ can be further simplified. In fact, in time interval $[\tau_1, \tau_2]$, $\beta_1(t) = \pi$, we have $\Omega_x(t) = \Omega_y(t) = 0$ according to Eq. (24). As a result, the system does not evolve in time interval $[\tau_1, \tau_2]$ as $H_s(t) = 0$. Therefore, the time interval $[\tau_1, \tau_2]$ can be reduced by letting $\tau_2 \to \tau_1$. In this case, we also have the change of geometric phase as

$$\Delta\Theta_- = \lim_{\tau_2\to\tau_1}[\Theta_-(\tau_2) - \Theta_-(\tau_1)] = \lim_{\tau_2\to\tau_1}\int_{\tau_1}^{\tau_2}\frac{\Theta_s dt}{\tau_2 - \tau_1} = \Theta_s. \tag{29}$$

Therefore, in the limit of $\tau_2 = \tau_1 = \tau$, we only need to increase $\beta_1(t)$ from 0 to π in time interval $[0, \tau]$ and set $\beta_1(t) = \beta_1[\tau(T - t)/(T - \tau)]$, $\beta_2(t) = -\Theta_s + \beta_2[\tau(T - $

$t)/(T - \tau)]$ in time interval $[\tau, T]$. Besides, as $\Omega_x(\tau) = \Omega_y(\tau) = 0$, the expressions of $\Omega_x(t)$ and $\Omega_y(t)$ can be still continuous functions if we make the value of β_2 increase by $-\Theta_s$ at the moment of $t = \tau$.

B. Selections of parameters for robust control

In Sec. IV, we have determined boundary conditions for parameters $\beta_1(t)$ and $\beta_2(t)$. However, specific expressions for $\beta_1(t)$ and $\beta_2(t)$ are still not given. In a real implementation of atomic quantum gates by using laser pulses, systematic errors of laser pulses due to imperfections of devices may be troublesome factors to obtain high gate fidelities. In order to realize robust control, let us now discuss selections of parameters $\beta_1(t)$ and $\beta_2(t)$ with the help of an optimal method [44] by nullifying systematic error sensitivity. In presence of the systematic error with error coefficient ϵ, the Rabi frequencies of laser pulses become $\Omega_{01}(t) \to (1 + \epsilon)\Omega_{01}(t)$, $\Omega_1(t) \to (1 + \epsilon)\Omega_1(t)$. According to Eq. (15), we have $\tilde{\Omega}_1(t) \to [2(1 + \epsilon)^2\bar{\Omega}_0(t)\bar{\Omega}_{01}(t)]/\Delta_1 = (1 + 2\epsilon)\tilde{\Omega}_1(t) + O(\epsilon^2)$, with $O(\epsilon^2)$ being the terms with orders equal to or higher than ϵ^2. Thus, in the effective Hamiltonian, the effective error coefficient is $\tilde{\epsilon} = 2\epsilon$, and the erroneous effective Hamiltonian is $\tilde{H}_s(t) = (1 + \tilde{\epsilon})H_s(t)$. With the help of time-dependent perturbation theory, one can derive [44,45]

$$\left|\psi_s^{\tilde{\epsilon}}(T)\right\rangle = |\psi_s(T)\rangle - i\tilde{\epsilon} \int_0^T dt\, U_s(T, t)H_s(t)|\psi_s(t)\rangle + O(\tilde{\epsilon}^2),$$
(30)

where $|\psi_s(t)\rangle$ ($|\psi_s^{\tilde{\epsilon}}(t)\rangle$) is the state of the system without (with) systematic errors. As the state $|r-\rangle_{01}$ is dynamically decoupled to the Hamiltonian $H_s(t)$, and the evolution with initial state $|r+\rangle_{01}$ is described by $|\psi_s(t)\rangle = e^{i\alpha_-(t)}|\phi_-(t)\rangle$, we estimate the fidelity as

$$F_s = 1 - \tilde{\epsilon}^2\left|\int_0^T e^{2i\alpha_-(t)}\langle\phi_+(t)|H_s(t)|\phi_-(t)\rangle dt\right|^2 + O(\tilde{\epsilon}^3),$$
(31)

with $\alpha_+(t) = -\alpha_-(t)$ being considered. Therefore, the systematic error sensitivity Q_s can be calculated as

$$Q_s = -\frac{\partial^2 F_s}{2\partial\tilde{\epsilon}^2} = \left|\int_0^T e^{i\chi(t)}\dot{\beta}_1 \sin^2\beta_1 dt\right|^2,$$
(32)

with $\chi(t) = \beta_2(t) + 2\alpha_-(t)$. To nullify Q_s, we consider $\chi(t) = \chi_0\{2\beta_1(t) - 2\sin[2\beta_1(t)]\}$ ($t \in [0, \tau)$) [44,46], with χ_0 being a time-independent parameter. Noticing that, at $t = \tau$, $\chi(t)$ have a shift as $\Delta\chi = \Delta\beta_2 + 2\Delta\Theta_- = \Theta_s$, one can derive $\chi(t) = \Theta_s + \chi_0\{2\beta_1(t) - \sin[2\beta_1(t)]\}$ ($t \in [\tau, T]$) and $Q_s = \sin^2(\chi_0\pi)\sin^2(\Theta_s/2)/\chi_0^2$ [see Fig. 3(a)]. Therefore, Q_s can be nullified when χ_0 is a nonzero integer $[Q_s \to \pi^2 \sin^2(\Theta_s/2), (\chi_0 \to 0)]$. Considering the fact that a larger value of χ_0 leads to a longer operation time when the maximal pulse intensity is fixed, we set $\chi_0 = 1$. In this case, we have $\beta_2(t) = 4\sin^3[\beta_1(t)]/3$ with $t \in [0, \tau)$ and $\beta_2(t) = -\Theta_s + 4\sin^3[\beta_1(t)]/3$ with $t \in [\tau, T]$. To make the pulses continuous and vanish at the boundary, we consider $\beta_1(t)$ as $\beta_1(t) = \pi \sin^2(\pi t/T)$ with $\tau = T/2$ being set.
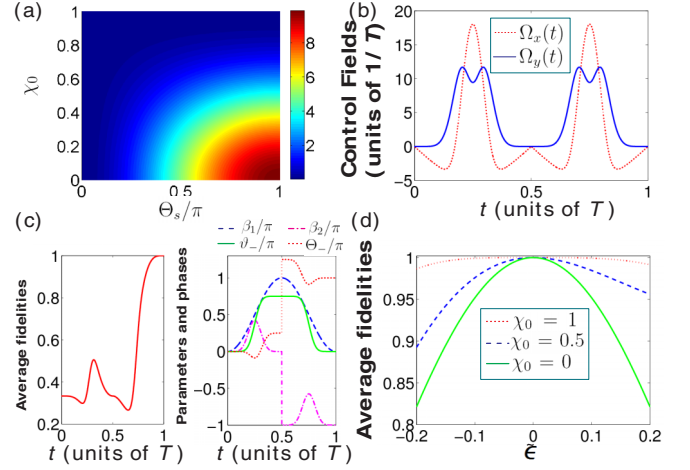

FIG. 3. (a) Q_s versus Θ_s/π and χ_0. (b) $\Omega_x(t)$ and $\Omega_y(t)$ versus t. (c) Average fidelities $\bar{F}_N(t)$, parameters $\beta_1(t)$, $\beta_2(t)$, and phases $\vartheta_-(t)$, $\Theta_-(t)$ in the implementation of the NOT gate versus t with the effective Hamiltonian. (d) The final average fidelities $\bar{F}_N(T)$ versus $\tilde{\epsilon}$ with the effective Hamiltonian and parameters $\chi_0 = 1$ (red dotted line), $\chi_0 = 0.5$ (blue dashed line), and $\chi_0 = 0$ (green solid line).

With the parameters designed above, we plot $\Omega_x(t)$ and $\Omega_y(t)$ versus t in Fig. 3(b), from which we can further obtain $\tilde{\Omega}_{max}^s = \max_{t\in[0,T]}[\tilde{\Omega}_1(t)] = 20.35/T$. Moreover, we plot the average fidelity (see Appendix D for details) of the implementation of the NOT gate versus t in Fig. 3(c) as an example to show the validity of the reverse engineering and the parameter selections discussed above. The average fidelity is defined as [92,93]

$$\bar{F}_N(t) = \frac{1}{\mathcal{N}(\mathcal{N} + 1)}\{\text{Tr}[M(t)M^\dagger(t)] + |\text{Tr}[M(t)]|^2\}, \quad (33)$$

with $M(t) = \mathcal{P}_c\tilde{U}_N^\dagger U_s(t)\mathcal{P}_c$, $\tilde{U}_N = |0r\rangle_{01}\langle 0r| + |r\rangle_0\langle r| \otimes U_N$, $\mathcal{P}_c = |r0\rangle_{01}\langle r0| + |r1\rangle_{01}\langle r1|$ being the projection operator onto the computational subspace, and $\mathcal{N} = 2$ for the two-dimensional computational subspace. As shown in Fig. 3(c), in accordance with the expectation, the average fidelity becomes unity at $t = T$. In addition, we also plot the variations of parameters $\beta_1(t)$, $\beta_2(t)$ and acquired dynamic phase $\vartheta_-(t)$ and geometric phase $\Theta_-(t)$ in Fig. 3(c), where we can find that the dynamic phase $\vartheta_-(t)$ finally vanishes at $t = T$, while the geometric phase reaches the preset value $\Theta_-(T) = \Theta_s = \pi$. This means we get a pure geometric phase in the process. Therefore, the reverse engineering and the parameter selections are effectively applied to the effective Hamiltonian $H_s(t)$ for the implementation of single qubit gates.

On the other hand, we plot the average fidelities $\bar{F}_N(T)$ at the final time T versus $\tilde{\epsilon}$ with $\chi_0 = 1$, $\chi_0 = 0.5$ and $\chi_0 = 0$ in Fig. 3(d) to show the robustness against systematic errors. According to the red dotted line in Fig. 3(d), $\bar{F}_N(T)$ stays higher than 0.9864 when $\tilde{\epsilon} \in [-0.2, 0.2]$ with $\chi_0 = 1$. This result shows that the implementation of the NOT gate with the optimal parameter $\chi_0 = 1$ is quite insensitive to systematic errors. We also see from the green solid line in Fig. 3(d) that the average fidelity falls to 0.8212 when $\tilde{\epsilon} = \pm 0.2$ with $\chi_0 = 0$. Noticing that when $\chi_0 = 0$ the implementation of the single qubit gate becomes the same as that in the conven-

tional NHQC with only σ_x control, the protocol can improve the robustness against systematic errors. Moreover, we see from the blue dashed line in Fig. 3(d) that the robustness against systematic errors with $\chi_0 = 0.5$ is between $\chi_0 = 0$ and $\chi_0 = 1$. As the total operation time increases with χ_0 when the maximal intensity of laser pulses is fixed, and the success probability of the protocol deceases with the increase of total operation time as shown in Sec. III B, one may adjust the value of χ_0 between 0 and 1 to make a tradeoff between the robustness against systematic errors and dissipation.

V. TWO-QUBIT ENTANGLING GATES

In this section, let us further study the implementations of two-qubit entangling gates. Based on the effective Hamiltonian $H_e(t)$ in Eq. (14), we consider the conditions $|\Omega_{e3}(t)| \gg \{|\Omega_{e1}(t)|, |\Omega_{e2}(t)|\}$, $\mu_3(t) = 0$, and $\dot{\tilde{\Omega}}_3(t) = 0$. H_{e_3} can be diagonalized as

$$H_{e_3} = \tilde{\Omega}_3(|\Phi_+\rangle\langle\Phi_+| - |\Phi_-\rangle\langle\Phi_-|), \quad (34)$$

with $|\Phi_\pm\rangle = (|0r+\rangle_{012} \pm |0+r\rangle_{012})/\sqrt{2}$. By performing a rotation transform with $\exp(-iH_{e_3}t)$, the effective Hamilto-

nian can be transformed into

$$\bar{H}_e(t) = \bar{H}_{e_0}(t) + \bar{H}_{e_1}(t) + \bar{H}_{e_2}(t),$$

$$\bar{H}_{e_0}(t) = \frac{\Omega_{e_1}(t)}{\sqrt{2}}|r++\rangle_{012}(\langle\Phi_+|e^{-i\tilde{\Omega}_3 t} + \langle\Phi_-|e^{i\tilde{\Omega}_3 t})$$

$$+ \frac{\Omega_{e_2}(t)}{\sqrt{2}}|r++\rangle_{012}(\langle\Phi_+|e^{-i\tilde{\Omega}_3 t} - \langle\Phi_-|e^{i\tilde{\Omega}_3 t}) + \text{H.c.}$$

$$\bar{H}_{e_1}(t) = \Omega_{e_1}(t)|r+-\rangle_{012}\langle 0r-| + \text{H.c.},$$

$$\bar{H}_{e_2}(t) = \Omega_{e_2}(t)|r-+\rangle_{012}\langle 0-r| + \text{H.c.} \quad (35)$$

After omitting terms with high oscillation frequencies $\pm\tilde{\Omega}_3$, the effective Hamiltonian can be simplified as

$$\bar{H}'_e(t) = \bar{H}_{e_1}(t) + \bar{H}_{e_2}(t),$$

$$\bar{H}_{e_1}(t) = \Omega_{e_1}(t)|r+-\rangle_{012}\langle 0r-| + \text{H.c.}, \quad (36)$$

$$\bar{H}_{e_2}(t) = \Omega_{e_2}(t)|r-+\rangle_{012}\langle 0-r| + \text{H.c.}$$

According to Eq. (36), evolutions in the subspaces $\mathcal{S}_1 = \text{span}\{|r+-\rangle_{012}, |0r-\rangle_{012}\}$ and $\mathcal{S}_2 = \text{span}\{|r-+\rangle_{012}, |0-r\rangle_{012}\}$ are independent, and the states $|r++\rangle_{012}$ and $|r--\rangle_{012}$ are dynamically decoupled to the effective Hamiltonian $\bar{H}'_e(t)$. Similarly to Eq. (19), we can make the following definitions:

$$\sigma_x^{(1)} = |0r-\rangle_{01}\langle r+-| + \text{H.c.}, \quad \sigma_y^{(1)} = -i|0r-\rangle_{01}\langle r+-| + \text{H.c.},$$

$$\sigma_z^{(1)} = |0r-\rangle_{01}\langle 0r| - |r+-\rangle_{01}\langle r+-|, \quad \sigma_x^{(2)} = |0-r\rangle_{01}\langle r-+| + \text{H.c.},$$

$$\sigma_y^{(2)} = -i|0-r\rangle_{01}\langle r-+| + \text{H.c.}, \quad \sigma_z^{(2)} = |0-r\rangle_{01}\langle 0r| - |r-+\rangle_{01}\langle r-+|, \quad (37)$$

which satisfy

$$[\sigma_x^{(j)}, \sigma_y^{(j)}] = 2i\sigma_z^{(j)}, \quad [\sigma_y^{(j)}, \sigma_z^{(j)}] = 2i\sigma_x^{(j)}, \quad [\sigma_z^{(j)}, \sigma_x^{(j)}] = 2i\sigma_y^{(j)}, \quad [\sigma_q^{(1)}, \sigma_{q'}^{(2)}] = 0 \ (q, q' = x, y, z). \quad (38)$$

Therefore, we can separately investigate evolutions in the subspaces $\mathcal{S}_1$ and $\mathcal{S}_2$ with su(2) algebra. Similarly to the process in Sec. IV A, we can derive an invariant $I_2(t)$ as

$$I_2(t) = \sum_{j=1,2} \sum_{q=x,y,z} \lambda_q^{(j)}(t)\sigma_q^{(j)}, \quad (39)$$

with

$$\lambda_x^{(j)}(t) = \sin\beta_1^{(j)} \sin\beta_2^{(j)}, \quad \lambda_y^{(j)}(t) = \sin\beta_1^{(j)} \cos\beta_2^{(j)}, \quad \lambda_z^{(j)}(t) = \cos\beta_1^{(j)}, \quad (40)$$

and eigenvectors of the dynamic invariant $I_2(t)$ are given by

$$|\phi_+^{(1)}(t)\rangle = \cos\frac{\beta_1^{(1)}}{2}|0r-\rangle_{01} + ie^{-i\beta_2^{(1)}}\sin\frac{\beta_1^{(1)}}{2}|r+-\rangle_{01},$$

$$|\phi_+^{(2)}(t)\rangle = \cos\frac{\beta_1^{(2)}}{2}|0-r\rangle_{01} + ie^{-i\beta_2^{(2)}}\sin\frac{\beta_1^{(2)}}{2}|r-+\rangle_{01},$$

$$|\phi_-^{(1)}(t)\rangle = ie^{i\beta_2^{(1)}}\sin\frac{\beta_1^{(1)}}{2}|0r-\rangle_{01} + \cos\frac{\beta_1^{(1)}}{2}|r+-\rangle_{01},$$

$$|\phi_-^{(2)}(t)\rangle = ie^{i\beta_2^{(2)}}\sin\frac{\beta_1^{(2)}}{2}|0-r\rangle_{01} + \cos\frac{\beta_1^{(2)}}{2}|r-+\rangle_{01}. \quad (41)$$

In addition, the time derivatives of dynamic phases and geometric phases acquired by $|\phi_\pm^{(j)}(t)\rangle$ can be respectively

calculated by

$$\dot{\vartheta}_\pm^{(j)}(t) = \mp\frac{\dot{\beta}_2^{(j)}\sin^2\beta_1^{(j)}}{2\cos\beta_1^{(j)}}, \quad \dot{\Theta}_\pm^{(j)}(t) = \pm\dot{\beta}_2^{(j)}\sin^2\frac{\beta_1^{(j)}}{2}. \quad (42)$$

By applying the parameter design of $\beta_1(t)$ and $\beta_2(t)$ in Sec. IV to parameters $\beta_1^{(j)}$ and $\beta_2^{(j)}$, evolutions with initial states $|r+-\rangle_{012}$ and $|r-+\rangle_{012}$ will move, cycling along $|\phi_-^{(1)}(t)\rangle$ and $|\phi_-^{(2)}(t)\rangle$ with geometric phases $\bar{\Theta}_1$ and $\bar{\Theta}_2$ acquired while the dynamic phases are eliminated. Then, the operation on computational atoms 1 and 2 reads

$$U_{12}(T, 0) = |++\rangle_{12}\langle ++| + e^{i\bar{\Theta}_1}|+-\rangle_{12}\langle +-|$$

$$+ e^{i\bar{\Theta}_2}|-+\rangle_{12}\langle -+| + |--\rangle_{12}\langle --|$$

$$= e^{-i\bar{\Theta}_1/2}|+\rangle_1\langle +| \otimes e^{-i\bar{\Theta}_1\vec{n}_2\cdot\vec{\sigma}_2/2} + e^{i\bar{\Theta}_2/2}|-\rangle_1\langle -|$$

$$\otimes e^{i\bar{\Theta}_2\vec{n}_2\cdot\vec{\sigma}_2/2}, \quad (43)$$

with $\vec{n}_2 = [\sin\theta_2\cos\varphi_2, \sin\theta_2\sin\varphi_2, \cos\theta_2]$, $\vec{\sigma}_2 = [\sigma_{x2}, \sigma_{y2}, \sigma_{z2}]$, $\sigma_{x2} = |0\rangle_2\langle 1| + \text{H.c.}$, $\sigma_{y2} = -i|0\rangle_2\langle 1| + \text{H.c.}$, and $\sigma_{z2} = |0\rangle_2\langle 0| - |1\rangle_2\langle 1|$. Equation (43) can be considered as a controlled arbitrary-angle-rotation gate for atom 2 with atom 1 being the control qubit. For example, when $(\bar{\Theta}_1, \bar{\Theta}_2, \theta_1, \varphi_1, \theta_2, \varphi_2) = \pi(0, 1, 0, 0, 1/2, 1)$, the operation on atoms 1 and 2 is a controlled-NOT (C-NOT) gate $U_{CN} = |0\rangle_1\langle 0| \otimes \mathbb{1}_2 + |1\rangle_1\langle 1| \otimes \sigma_{x2}$, with $\mathbb{1}_2$ being the identity operation for atom 2; when $(\bar{\Theta}_1, \theta_1, \varphi_1, \theta_2) = \pi(0, 0, 0, 1)$, the controlled-$\bar{\Theta}_2$-phase gate of atoms 1 and 2 as $U_{C\bar{\Theta}_2} = |0\rangle_1\langle 0| \otimes \mathbb{1}_2 + |1\rangle_1\langle 1| \otimes \text{diag}[1, e^{i\bar{\Theta}_2}]_2$ is realized.

VI. NUMERICAL ANALYSIS AND DISCUSSIONS

A. Numerical analysis of single-qubit gate

Let us now analyze the evolution based on the full Hamiltonian $H(t)$ in Eq. (A1). First, we check the performance of the single-qubit gate by taking the NOT gate as an example. To make the Rydberg blockade and effective Hamiltonian valid, we choose $V = 7200/T$ and $\Delta_1 = 360/T$. Considering a reported Rydberg interaction strength $V = 2\pi \times 50$ MHz [94–96], where the center-to-center distance between Rydberg atoms is about $d = 3.755$ μm with van der Waals coefficient $C_6^s(r, r) = 8.8 \times 10^{11}$ μm^6/s [97,98], the total interaction time is $T = 22.9$ μs, which gives the success probability as $P_s = 99.74\%$ for probing state $|r\rangle_0$ of the auxiliary atom. Furthermore, although the Stark shift $-2V(\bar{\Omega}_1^2|r+\rangle_{01}\langle r+| + \bar{\Omega}_{01}^2|0r\rangle_{01}\langle 0r|)/(V^2 - \Delta_1^2)$ due to the second-order perturbation can be neglected when $V \gg \Delta_1$, we can still eliminate the Stark shift by using auxiliary pulses or levels [88,95] to loosen the requirement on the ratio between V and Δ_1. We plot the average fidelity $\bar{F}_N(t)$ versus t with the full Hamiltonian in Fig. 4(a). From Fig. 4(a), up to small oscillations, the curve matches well with that plotted in Fig. 3(c) with the effective Hamiltonian. The final average fidelity $\bar{F}_N(T)$ is 0.9943. Thus, the considered Rydberg interaction strength V and the detuning Δ_1 are proper for the construction of the effective Hamiltonian. In general, one may increase the ratios $\tilde{\Omega}_{\max}^s/\Delta_1$ and Δ_1/V to further improve the fidelity. However, the total interaction time would also increase, and the successful probability P_s would reduce due to decays of atoms from Rydberg states.

As the approximation made for the effective Hamiltonian also causes some errors in the operation, we here investigate the robustness against systematic errors of the implementation of the NOT gate with the full Hamiltonian. The final average fidelities $\bar{F}_N(T)$ versus ϵ with $\chi_0 = 1$, $\chi_0 = 0.5$, and $\chi_0 = 0$ are plotted in Fig. 4(b) based on the evolution governed by the full Hamiltonian. We can see from the red dotted line in Fig. 4(b) that, when $\epsilon \in [-0.1, 0.1]$ (corresponding to $\tilde{\epsilon} \in [-0.2, 0.2]$), the average fidelity with $\chi_0 = 1$ stays higher than 0.988. Therefore, the robustness against systematic errors is inherited when the full dynamics is considered. Moreover, as seen from the green solid line and the blue dashed line in Fig. 4(b), the average fidelities with $\chi_0 = 0$ and $\chi_0 = 0.5$ are much more sensitive to systematic errors. For example, for $\chi_0 = 0$, the average fidelity is only $\bar{F}_N(T) = 0.8089$ when $\epsilon = 0.1$.
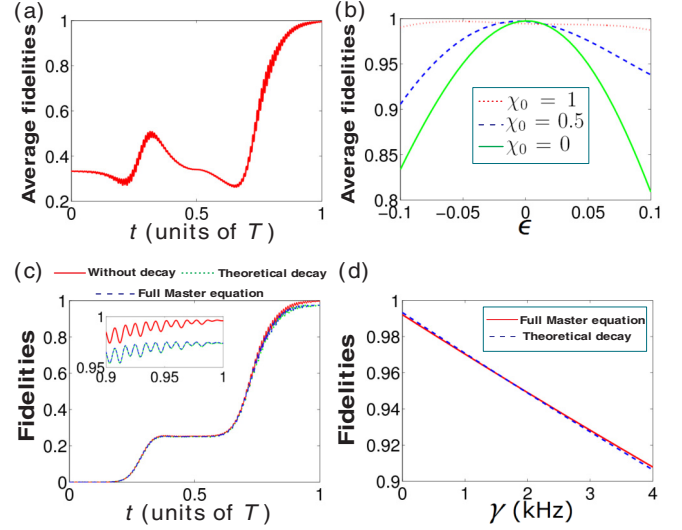

FIG. 4. (a) Average fidelities $\bar{F}_N(t)$ of the implementation of the NOT gate versus t with the full Hamiltonian. (b) The final average fidelities $\bar{F}_N(T)$ versus ϵ with the full Hamiltonian and parameters $\chi_0 = 1$ (red-dotted line), $\chi_0 = 0.5$ (blue-dashed line) and $\chi_0 = 0$ (green-solid line). (c) Fidelities $F_N(t)$ of the implementation of the NOT gate versus t calculated by the master equation with initial state $|r0\rangle_{01}$. Red-solid line: $\gamma = 0$, green-dotted line: $\gamma = 1$ kHz with theoretical result in Eq. (17), blue-dashed line: $\gamma = 1$ kHz with the full master equation. (d) Final fidelities $F_N(T)$ of the implementation of the NOT gate versus decay rate γ with initial state $|r0\rangle_{01}$ by using theoretical result in Eq. (17) (blue-dashed line) and the full master equation (red-solid line).

In the end of this section, let us study the influence of dissipation with the full Hamiltonian. As the evolution is not unitary when dissipation taken into account, we consider the evolution with the initial state $|r0\rangle_{01}$ as example to show evolution governed by the master equation. We plot the fidelity of the evolution before measuring the state of the auxiliary atom as $F_N(t) = \text{Tr}[U_N\rho(0)U_N^\dagger\rho(t)]$ versus t in Fig. 4(c). As shown by the red solid line in Fig. 4(c), the final fidelity without the decay is $F_N(T)|_{\gamma=0} = 0.9933$. In addition, the green dotted line points out that the final fidelity calculated by Eq. (17) with $\gamma = 1$ kHz is $\tilde{F}_N(T)|_{\gamma=1\,\text{kHz}} = \exp(-\gamma T)|_{\gamma=1\,\text{kHz}} \times F_N(T)|_{\gamma=0} = 0.9708$. Moreover, the blue dashed line indicates the final fidelity given by the full master equation [replacing the effective Hamiltonian $H_e(t)$ in Eq. (16) by the full Hamiltonian $H(t)$] with $\gamma = 1$ kHz is $F_N(T)|_{\gamma=1\,\text{kHz}} = 0.9704$, which is in accordance with the theoretical result $\tilde{F}_N(T)|_{\gamma=1\,\text{kHz}}$. Moreover, by comparing the green dotted line and the blue dashed line, we can also find that the dynamics governed by the full master equation matches well with that discussed in Sec. III B in the twelve-dimensional subspace. The result also proves that the theoretical analysis of the effective Hamiltonian and the subspace is valid. In Fig. 4(d), we consider the fidelity with a broader range of decay rate γ, where the fidelity obtained from full master equation is a little higher than that estimated from Eq. (17) when dissipation is relatively strong. This is because dissipation also restrains the population of $|rr\rangle_{01}$ alongside the Rydberg blockade. When γ reaches 4 kHz, the obtained

TABLE I. Success probability P_s, fidelity F_N', and purity ϱ_1 with different decay rates.

	γ (kHz)				
	0	1	2	3	4
P_s	0.9988	0.9770	0.9557	0.9348	0.9144
F_N'	0.9933	0.9932	0.9931	0.9930	0.9929
ϱ_1	1.0000	0.9998	0.9996	0.9993	0.9991

fidelity is 0.9079, still higher than 0.9. Therefore, the protocol holds robustness against dissipation. We also examine the probability successfully measuring the Rydberg state of the auxiliary atom as $P_s = \text{Tr}[\mathcal{P}_r \rho(T)]$ with the projection operator $\mathcal{P}_r = |r\rangle_0 \langle r| \otimes \mathbb{1}_1$ ($\mathbb{1}_1$ is the identity operator for computational atom 1), and the result is shown in Table I. Furthermore, the fidelity after successful measurement of the auxiliary atom and the purity of the density operator of computational atom 1 as $F_N' = \text{Tr}[\mathcal{P}_r \rho(T) \mathcal{P}_r U_N \rho(0) U_N^\dagger]/P_s$ and $\varrho_1 = \text{Tr}[\mathcal{P}_r \rho(T) \mathcal{P}_r \rho(T)]/P_s^2$ are also investigated, respectively. According to the data in Table I, although the success probability decreases when the decay rate increases, after successful measurement of the auxiliary atom, the fidelity of the NOT gate and the purity of the density operator of atom 1 are changed very slightly. Even when $\gamma = 4$ kHz, the fidelity F_N' is only reduced about 0.0004, and the purity ϱ_1 is still 0.9991. Therefore, by using the protocol, we can still obtain nearly perfect unitary evolution in the presence of dissipation if the measurement result of the state of the auxiliary atom is $|r\rangle_0$, which accords with the theoretical analysis in Sec. III B.

B. Numerical analysis of a two-qubit entangling gate

We now make a numerical analysis of a two-qubit entangling gate. As an example to show the implementation of a two-qubit entangling gate, we amply analyze the realization of the C-NOT gate in the following discussions. In this case, we switch off laser pulses $\Omega_1(t)$, $\Omega_1'(t)$, $\Omega_{01}(t)$, $\Omega_{01}'(t)$, $\Omega_{23}(t)$, and $\Omega_{23}'(t)$ for $\Omega_{e_1}(t) = 0$ and $\theta_1 = 0$. Besides, the waveform of $\Omega_{e2}(t)$ is considered as discussed in Sec. IV with invariant-based reverse engineering and the systematic-error-sensitivity nullification method. To meet the condition $\tilde{\Omega}_3 \gg |\Omega_{e2}(t)|$, we consider $\tilde{\Omega}_3 = 100/T$. Moreover, the Rydberg interaction strength and detunings are set as $V = 27000/T$, $\Delta_2 = 360/T$, and $\Delta_3 = 1500/T$ to build up the effective Hamiltonian. In this case, the total operation time is 85.94 μs with $V = 2\pi \times 50$ MHz, and the success probability is $P_s = 91.76\%$ with $\gamma = 1$ kHz. In addition, we eliminate the Stark shifts as

$$-\frac{2V}{V^2 - \Delta_2^2} \big[\bar{\Omega}_2^2 (|r \pm\rangle_{012}\langle r \pm| + |0r+\rangle_{012}\langle 0r+|)$$
$$+ \bar{\Omega}_{02}^2 (|0r\pm\rangle_{012}\langle 0r\pm| + |0 \pm r\rangle_{012}\langle 0 \pm r|) \big],$$
$$-\frac{2V}{V^2 - \Delta_3^2} \big[\bar{\Omega}_{13}^2 (|r + \pm\rangle_{012}\langle r + \pm| + |0 + r\rangle_{012}\langle 0 + r|)$$
$$+ \bar{\Omega}_{23}^2 (|r \pm +\rangle_{012}\langle r \pm +| + |0r+\rangle_{012}\langle 0r+|) \big], \quad (44)$$

(a) (b)

(c) Without decay — Theoretical decay ⋯⋯ — — Full Master equation — — (d)
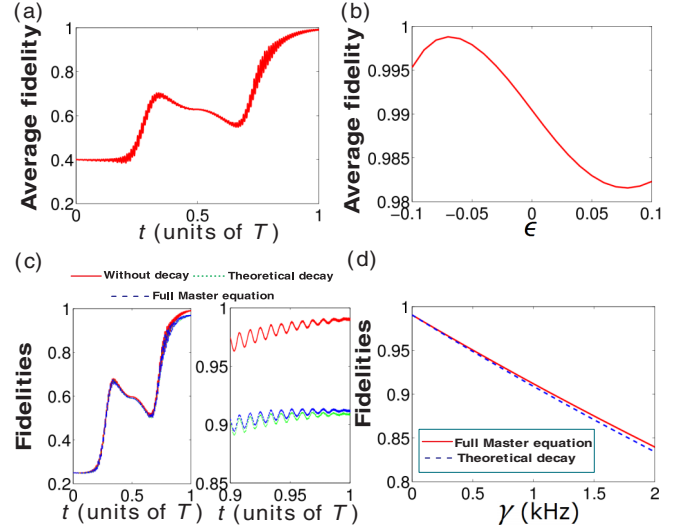
FIG. 5. (a) Average fidelity $\bar{F}_{CN}(t)$ of the implementation of the C-NOT gate versus t with the full Hamiltonian. (b) The final average fidelities $\bar{F}_{CN}(T)$ versus ϵ. (c) Fidelities $F_{CN}(t)$ of the implementation of the C-NOT gate versus t calculated by the master equation with initial state $(|r00\rangle_{012} + |r10\rangle_{012})/\sqrt{2}$. Red solid line: $\gamma = 0$; green dotted line: $\gamma = 1$ kHz with theoretical result in Eq. (17); blue-dashed line: $\gamma = 1$ kHz with the full master equation. (d) Final fidelities $F_{CN}(T)$ of the implementation of the C-NOT gate versus decay rate γ with initial state $(|r00\rangle_{012} + |r10\rangle_{012})/\sqrt{2}$ by using the theoretical result in Eq. (17) (blue dashed line) and the full master equation (red solid line).

by using auxiliary pulses [88,95]. The average fidelity of the implementation of the C-NOT gate is defined as [92,93]

$$\bar{F}_{CN}(t) = \frac{1}{\mathcal{N}'(\mathcal{N}'+1)} \{ \text{Tr}[M'(t)M'^\dagger(t)] + |\text{Tr}[M'(t)]|^2 \}, \quad (45)$$

with $M'(t) = |r\rangle_0\langle r| \otimes U_{CN} + |0\rangle_0\langle 0| \otimes \mathbb{1}_{12}$ and $\mathcal{N}' = 4$ being the dimension of the computational subspace. We plot $\bar{F}_{CN}(t)$ versus t in Fig. 5(a) and obtain the average fidelity of the implementation of the C-NOT gate as $\bar{F}_{CN}(T) = 0.9904$ at $t = T$. Therefore, the C-NOT gate can be successfully realized with the protocol.

We also check the robustness of the implementation of the C-NOT gate against systematic errors of laser pulses. The final average fidelity $\bar{F}_{CN}(T)$ of the implementation of the C-NOT gate versus error coefficient ϵ is plotted in Fig. 5(b). Seen from Fig. 5(b), $\bar{F}_{CN}(T)$ is always higher than 0.9823 when $\epsilon \in [-0.1, 0.1]$. Therefore, the implementation of the C-NOT gate is also insensitive to systematic errors. Moreover, we can also see from Fig. 5(b) that errors with $\epsilon > 0$ may decrease the average fidelity $\bar{F}_{CN}(T)$ in a range. However, in contrast, the errors with $\epsilon < 0$ may increase the average fidelity $\bar{F}_{CN}(T)$ in a range. This is because the satisfaction of the condition $\tilde{\Omega}_3 \gg \tilde{\Omega}_{e_2}(t)$ becomes worse when $\epsilon > 0$. Although the deviations of $\Omega_{e_2}(t)$ and $\Omega_{e_3}(t)$ are both about 2ϵ compared to the original ones according to Eq. (15), according to the second-order perturbation theory, the coefficients of error terms caused by the terms with high-frequency oscillations is approximately increased from $\Omega_{e_2}^2(t)/\tilde{\Omega}_3$ to $(1 + 2\epsilon)^2 \Omega_{e_2}^2(t)/[(1 + 2\epsilon)\tilde{\Omega}_3] = (1 + 2\epsilon)\Omega_{e_2}^2(t)/\tilde{\Omega}_3$. There-

TABLE II. Success probability P_s', fidelity F_{CN}', and purity ϱ_{12} with different decay rates.

	γ (kHz)		
	0	1	2
P_s'	0.9911	0.9130	0.8411
F_{CN}'	0.9992	0.9987	0.9981
ϱ_{12}	0.9995	0.9983	0.9971

fore, when $\epsilon < 0$, the parts of error caused by the approximation $\tilde{\Omega}_3 \gg \tilde{\Omega}_{e_2}(t)$ are compensated by systematic errors. The maxima of $\bar{F}_{CN}(T) = 0.9988$ appears at $\epsilon = -0.07$, which may be considered as a correction in the design of pulses for higher fidelity.

Finally, we check the performance of the protocol under the influence of dissipation by considering the initial state $(|r00\rangle_{012} + |r10\rangle_{012})/\sqrt{2}$ in the evolution governed by the master equation. We plot the fidelity of the evolution before measuring the state of the auxiliary atom as $F_{CN}(t) = \text{Tr}[U_{CN}\rho(0)U_{CN}^\dagger\rho(t)]$ versus t in Fig. 5(c). As seen from the red solid line in Fig. 5(c), the fidelity of the implementation of the C-NOT gate is $F_{CN}(T)|_{\gamma=0} = 0.9904$ at $t = T$. Moreover, the green dotted line in Fig. 4(c) is the fidelity calculated by Eq. (17) with $\gamma = 1$ kHz, which gives $\tilde{F}_{CN}(T)|_{\gamma=1\,\text{kHz}} = \exp(-\gamma T)|_{\gamma=1\,\text{kHz}} \times F_N(T)|_{\gamma=0} = 0.9089$. In addition, the blue-dashed line indicates that the final fidelity obtained by the full master equation is $F_{CN}(T)|_{\gamma=1\,\text{kHz}} = 0.9115$. We also plot the final fidelity $F_{CN}(T)$ of the implementation of the C-NOT gate with the initial state $(|r00\rangle_{012} + |r10\rangle_{012})/\sqrt{2}$ versus decay rate γ in Fig. 5(d), where one can also find that the final fidelity $F_{CN}(T)$ plotted by the full master equation is higher than the theoretical result obtained by Eq. (17) when the dissipation is relatively strong. This is because populations of states with multiple atoms in Rydberg states are restrained by dissipation. In the implementation of the two-qubit gate, the fidelity decreases more significantly compared with the result in the implementation of the single-qubit gate when dissipation is taken into account due to the increase of the total operation time. However, by measuring the state of the auxiliary atom, the influence of dissipation can be removed if the result is $|r\rangle_0$. Here, we define the success probability of getting the result $|r\rangle_0$ as $P_s' = \text{Tr}[\mathcal{P}_r'\rho(T)]$ with $\mathcal{P}_r' = |r\rangle_0\langle r| \times \mathbb{1}_{12}$. Furthermore, the fidelity of the C-NOT gate and the purity of the density operator of the computational atoms 1 and 2 after successful measurement of the auxiliary atom are defined as $F_{CN}' = \text{Tr}[\mathcal{P}_r'\rho(T)\mathcal{P}_r'U_{CN}\rho(0)U_{CN}^\dagger]/P_s$ and $\varrho_{12} = \text{Tr}[\mathcal{P}_r'\rho(T)\mathcal{P}_r'\rho(T)]/P_s'^2$, respectively. We calculate P_s', F_{CN}', and ϱ_{12} with some samples shown in Table II. According to the data in Table II, although the success probability P_s' decreases with the increase of the decay rate γ, the fidelity F_{CN}' and the purity ϱ_{12} in the case of successful measurement are almost unchanged. For example, when $\gamma = 1$ kHz, the decreases of F_{CN}' and ϱ_{12} are only 0.0005 and 0.0012, respectively. In addition, the measurement of state $|r\rangle_0$ can also help to reduce the effect of systematic errors and errors caused by the approximation, because these errors would also make the final state of the auxiliary atom deviate from $|r\rangle_0$. For example, when $\gamma = 0$, compared with the fidelity $F_{CN}(T)|_{\gamma=0} = 0.9904$ obtained without the measurement of

the auxiliary atom, the fidelity after successful measurement is improved to $F_{CN}' = 0.9992$. From the results above, the protocol is helpful to maintain a nearly perfect two-qubit unitary operation in the dissipative environment.

VII. CONCLUSION

In conclusion, we have proposed a protocol to realize atomic nonadiabatic holonomic quantum computation (NHQC) in the regime of Rydberg blockade. Assisted by the strong interaction between Rydberg atoms, the effective Hamiltonian was built up by the second-order perturbation theory with proper detunings. Based on the derived effective Hamiltonian, we further designed the laser pulses with the help of invariant-based reverse engineering. The advantages of invariant-based reverse engineering in NHQC have been shown in the protocol. On one hand, eigenvectors of the dynamic invariant provide natural evolution paths for NHQC. On the other hand, invariant-based reverse engineering is also compatible with the systematic-error-sensitivity nullification method, which makes the evolution insensitive to systematic errors of laser pulses. Generally, there are many different choices for the parameters in the nullification of systematic error sensitivity Q_s. In the implementation of a single- or two-qubit gate, by nullifying the systematic error sensitivity Q_s, we can derive optimal solutions for Rabi frequencies of laser pulses that can make the implementation insensitive to the systematic errors of pulses. Therefore, in the implementation of a general quantum circuit composed of a sequence of single- and two-qubit gates, we need to individually derive the Rabi frequencies of pulses with Q_s being nullified for each gate in the sequence. As a result, we can obtain a sequence of Rabi frequencies of pulses for each step of operations. In this way, we make the total systematic error sensitivity Q_s nullified in the whole process, so that the implementation of the quantum circuit maintains a high level when there exist systematic errors. Moreover, in the design of pulses, by setting proper boundary conditions for the time derivatives of control parameters, we can make each pulse in the sequence vanish at the final time of each step. Pulses in each two adjacent steps can be connected as a composite pulse described by a continuous function. Therefore, the composite pulse does not involve sudden changes in the whole process. In a real implementation, we just need to apply the composite pulse to the system. In addition, we analyzed the evolution in a dissipative environment based on the master equation. Both the theoretical and numerical results showed that the protocol can realize nearly perfect unitary operations if the auxiliary atom in the Rydberg state is successfully measured. Considering a typical decay rate $\gamma = 1$ kHz of a Rydberg state, the protocol produces acceptable success probabilities of measurements as 0.9770 and 0.9130 for single- and two-qubit gates, respectively. Compared with the previous Rydberg-atom-based NHQC protocol [64], the protocol has several advantages. First, with the invariant-based reverse engineering in the protocol, we obtain an invariant of the system whose eigenvectors can be used as paths for NHQC by only eliminating the acquired dynamic phases. This makes the parameter selections more convenient compared with that in the protocol of Ref. [64], where both the parallel transport conditions and

the unavailable couplings should be considered. Second, as a result of the convenience of parameter selections, the protocol can incorporate the systematic-error-sensitivity nullification method. This makes the protocol maintain high fidelities when systematic errors appear. Third, the system in the protocol of [64] will be in a mixed state when dissipation exists, while in the current protocol, as the heralded implementation is considered, the state of the system nearly maintains a pure state with successful measurement on the auxiliary atom. As the protocol is fully compatible with the advantages of geometric phases, reverse engineering, the systematic-error-sensitivity nullification method, heralded implementation, and Rydberg interaction, we hope the protocol can be helpful for precise quantum computation in a dissipative environment.

APPENDIX A: DERIVATIONS OF THE EFFECTIVE HAMILTONIAN

For the atomic system shown in Sec. III A, the Hamiltonian of the whole system under the rotating-wave approximation reads

$$H(t) = H_1(t) + H_2(t) + H_3(t) + H_v,$$

$$H_1(t) = \sum_{j,k=1}^{2} [\Omega_{kj}(t)e^{i\Delta_k t} + \Omega'_{kj}(t)e^{-i\Delta_k t}]|j-1\rangle_k\langle r| + \text{H.c.},$$

$$H_2(t) = \sum_{k=1}^{2} [\Omega_{0k}(t)e^{i\Delta_k t} + \Omega'_{0k}(t)e^{-i\Delta_k t}]|0\rangle_0\langle r| + \text{H.c.},$$

$$H_3(t) = \sum_{j,k=1}^{2} [\Omega_{kj3}(t)e^{i\Delta_3 t} + \Omega'_{kj3}(t)e^{-i\Delta_3 t}]|j-1\rangle_k\langle r| + \text{H.c.},$$

$$H_v = V(|rr\rangle_{01}\langle rr| + |rr\rangle_{02}\langle rr| + |rr\rangle_{12}\langle rr|). \tag{A1}$$

With the assumptions in Eq. (12), the Hamiltonian in Eq. (A1) can be rewritten as

$$H(t) = H_1(t) + H_2(t) + H_3(t) + H_v,$$

$$H_1(t) = \sum_{k=1}^{2} [\Omega_k(t)e^{i\Delta_k t} + \Omega'_k(t)e^{-i\Delta_k t}]|+\rangle_k\langle r| + \text{H.c.},$$

$$H_2(t) = \sum_{k=1}^{2} [\Omega_{0k}(t)e^{i\Delta_k t} + \Omega'_{0k}(t)e^{-i\Delta_k t}]|0\rangle_0\langle r| + \text{H.c.},$$

$$H_3(t) = \sum_{k=1}^{2} [\Omega_{k3}(t)e^{i\Delta_3 t} + \Omega'_{k3}(t)e^{-i\Delta_3 t}]|+\rangle_k\langle r| + \text{H.c.},$$

$$H_v = V(|rr\rangle_{01}\langle rr| + |rr\rangle_{02}\langle rr| + |rr\rangle_{12}\langle rr|). \tag{A2}$$

In Eq. (A2), $|+\rangle_k$ reads $|+\rangle_k = \cos(\theta_k/2)|0\rangle_k + \sin(\theta_k/2)e^{i\varphi_k}|1\rangle_k$, and it has an orthogonal partner as $|-\rangle_k = \sin(\theta_k/2)|0\rangle_k - \cos(\theta_k/2)e^{i\varphi_k}|1\rangle_k$. We assume that the system works at the Rydberg blockade regime with $V \gg \{\Delta_k, \Delta_3, |\Omega_k(t)|, |\Omega'_k(t)|, |\Omega_{0k}(t)|, |\Omega'_{0k}(t)|, |\Omega_{k3}(t)|, |\Omega'_{k3}(t)|\}$. The Hamiltonian in the rotating frame of $U_0(t) = \exp(-iH_v t)$ can be derived as

$$\tilde{H}(t) = \tilde{H}_1(t) + \tilde{H}_2(t) + \tilde{H}_3(t),$$

$$\tilde{H}_1(t) = [\Omega_1(t)e^{i\Delta_1 t} + \Omega'_1(t)e^{-i\Delta_1 t}](|0++\rangle_{012}\langle 0r+| + |0+-\rangle_{012}\langle 0r-|)$$
$$+ [\Omega_2(t)e^{i\Delta_2 t} + \Omega'_2(t)e^{-i\Delta_2 t}](|0++\rangle_{012}\langle 0+r| + |0-+\rangle_{012}\langle 0-r|) + \text{H.c.},$$

$$\tilde{H}_2(t) = \sum_{k=1}^{2}\sum_{J,J'=\pm} [\Omega_{0k}(t)e^{i\Delta_k t} + \Omega'_{0k}(t)e^{-i\Delta_k t}]|0JJ'\rangle_{012}\langle rJJ'| + \text{H.c.},$$

$$\tilde{H}_3(t) = [\Omega_{13}(t)e^{i\Delta_3 t} + \Omega'_{13}(t)e^{-i\Delta_3 t}](|0++\rangle_{012}\langle 0r+| + |0+-\rangle_{012}\langle 0r-|)$$
$$+ [\Omega_{23}(t)e^{i\Delta_3 t} + \Omega'_{23}(t)e^{-i\Delta_3 t}](|0++\rangle_{012}\langle 0+r| + |0-+\rangle_{012}\langle 0-r|) + \text{H.c.}, \tag{A3}$$

by omitting the terms with oscillation frequencies in the scale of V. To further simplify the dynamics of the system, we consider the condition $\{\Delta_k, \Delta_3, |\Delta_1 - \Delta_2|, |\Delta_1 - \Delta_3|, |\Delta_2 - \Delta_3|\} \gg \{|\Omega_k(t)|, |\Omega'_k(t)|, |\Omega_{0k}(t)|, |\Omega'_{0k}(t)|, |\Omega_{k3}(t)|, |\Omega'_{k3}(t)|\}$. With the help of the second-order perturbation theory [99], the effective Hamiltonian is derived as

$$H_e(t) = H_{e_0}(t) + H_{e_1}(t) + H_{e_2}(t) + H_{e_3}(t),$$

$$H_{e_0}(t) = \Omega_{e_1}(t)|r++\rangle_{012}\langle 0r+|$$
$$+ \Omega_{e_2}(t)|r++\rangle_{012}\langle 0+r| + \text{H.c.}$$

$$H_{e_1}(t) = \Omega_{e_1}(t)|r+-\rangle_{012}\langle 0r-| + \text{H.c.},$$

$$H_{e_2}(t) = \Omega_{e_2}(t)|r-+\rangle_{012}\langle 0-r| + \text{H.c.},$$

$$H_{e_3}(t) = \Omega_{e_3}(t)|0r+\rangle_{012}\langle 0+r| + \text{H.c.} \tag{A4}$$

with

$$\Omega_{e_k}(t) = \frac{\Omega'_k(t)\Omega'^*_{0k}(t) - \Omega_k(t)\Omega^*_{0k}(t)}{\Delta_k},$$

$$\Omega_{e_3}(t) = \frac{\Omega'_{13}(t)\Omega'^*_{23}(t) - \Omega_{13}(t)\Omega^*_{23}(t)}{\Delta_3}. \tag{A5}$$

TABLE III. Basis vector of subspace $\mathcal{B}'$.

$|\Phi_1\rangle$	$|\Phi_2\rangle$	$|\Phi_3\rangle$	$|\Phi_4\rangle$
$|r++\rangle_{012}$	$|r+-\rangle_{012}$	$|r-+\rangle_{012}$	$|r--\rangle_{012}$
$|\Phi_5\rangle$	$|\Phi_6\rangle$	$|\Phi_7\rangle$	$|\Phi_8\rangle$
$|0r+\rangle_{012}$	$|0r-\rangle_{012}$	$|0+r\rangle_{012}$	$|0-r\rangle_{012}$
$|\Phi_9\rangle$	$|\Phi_{10}\rangle$	$|\Phi_{11}\rangle$	$|\Phi_{12}\rangle$
$|0++\rangle_{012}$	$|0+-\rangle_{012}$	$|0-+\rangle_{012}$	$|0--\rangle_{012}$

With the assumptions in Eq. (13), $\Omega_{e_k}(t)$ can be simplified as

$$\Omega_{e_k}(t) = \frac{2\bar{\Omega}_k(t)\bar{\Omega}_{0k}(t)}{\Delta_k} \sin\left(\frac{\mu_k - \mu_k'}{2}\right) e^{i(\mu_k' + \mu_k + \pi)/2},$$

$$\Omega_{e_3}(t) = \frac{2\bar{\Omega}_{13}(t)\bar{\Omega}_{23}(t)}{\Delta_k} \sin\left(\frac{\mu_3 - \mu_3'}{2}\right) e^{i(\mu_3' + \mu_3 + \pi)/2}. \quad \text{(A6)}$$

Considering $\mu_k - \mu_k' = \pi$ and $\mu_3 - \mu_3' = \pi$, we have $\Omega_{e_k}(t) = \tilde{\Omega}_k(t)e^{i\mu_k(t)}$, $\Omega_{e_3}(t) = \tilde{\Omega}_3(t)e^{i\mu_3(t)}$ with

$$\tilde{\Omega}_k(t) = \frac{2\bar{\Omega}_k(t)\bar{\Omega}_{0k}(t)}{\Delta_k}, \qquad \tilde{\Omega}_3(t) = \frac{2\bar{\Omega}_{13}(t)\bar{\Omega}_{23}(t)}{\Delta_3}. \quad \text{(A7)}$$

APPENDIX B: MATRIX ELEMENTS OF THE TIME DERIVATIVE OF THE DENSITY OPERATOR

For simplicity, we number the basis vectors of subspace $\mathcal{B}'$ in Table III.

According to Eq. (16), the time derivatives of nonzero matrix elements of $\rho(t)$ can be calculated as

$$\dot{\rho}_{1,1} = -i\Omega_{e_1}\rho_{5,1} + i\Omega_{e_1}^*\rho_{1,5} - i\Omega_{e_2}\rho_{7,1} + i\Omega_{e_2}^*\rho_{1,7} - \gamma\rho_{1,1},$$

$$\dot{\rho}_{1,2} = -\gamma\rho_{1,2}, \quad \dot{\rho}_{1,3} = -\gamma\rho_{1,3}, \quad \dot{\rho}_{1,4} = -\gamma\rho_{1,4},$$

$$\dot{\rho}_{1,5} = i\Omega_{e_1}(\rho_{1,1} - \rho_{5,5}) - \gamma\rho_{1,5}, \quad \dot{\rho}_{1,6} = -\gamma\rho_{1,6},$$

$$\dot{\rho}_{1,7} = i\Omega_{e_2}(\rho_{1,1} - \rho_{7,7}) - \gamma\rho_{1,7}, \quad \dot{\rho}_{1,8} = -\gamma\rho_{1,8},$$

$$\dot{\rho}_{2,1} = -\gamma\rho_{2,1}, \quad \dot{\rho}_{2,2} = -i\Omega_{e_1}\rho_{6,2} + i\Omega_{e_1}^*\rho_{2,6} - \gamma\rho_{2,2},$$

$$\dot{\rho}_{2,3} = -\gamma\rho_{2,3}, \quad \dot{\rho}_{2,4} = -\gamma\rho_{2,4}, \quad \dot{\rho}_{2,5} = -\gamma\rho_{2,5},$$

$$\dot{\rho}_{2,6} = i\Omega_{e_1}(\rho_{2,2} - \rho_{6,6}) - \gamma\rho_{2,6}, \quad \dot{\rho}_{2,7} = -\gamma\rho_{2,7}, \quad \dot{\rho}_{2,8} = -\gamma\rho_{2,8},$$

$$\dot{\rho}_{3,1} = -\gamma\rho_{3,1}, \quad \dot{\rho}_{3,2} = -\gamma\rho_{3,2}, \quad \dot{\rho}_{3,3} = -i\Omega_{e_2}\rho_{8,3} + i\Omega_{e_2}^*\rho_{3,8} - \gamma\rho_{3,3}$$

$$\dot{\rho}_{3,4} = -\gamma\rho_{3,4}, \quad \dot{\rho}_{3,5} = -\gamma\rho_{3,5}, \quad \dot{\rho}_{3,6} = -\gamma\rho_{3,6},$$

$$\dot{\rho}_{3,7} = -\gamma\rho_{3,7}, \quad \dot{\rho}_{3,8} = i\Omega_{e_2}(\rho_{3,3} - \rho_{8,8}) - \gamma\rho_{3,8},$$

$$\dot{\rho}_{4,1} = -\gamma\rho_{4,1}, \quad \dot{\rho}_{4,2} = -\gamma\rho_{4,2}, \quad \dot{\rho}_{4,3} = -\gamma\rho_{4,3}, \quad \dot{\rho}_{4,4} = -\gamma\rho_{4,4},$$

$$\dot{\rho}_{4,5} = -\gamma\rho_{4,5}, \quad \dot{\rho}_{4,6} = -\gamma\rho_{4,6}, \quad \dot{\rho}_{4,7} = -\gamma\rho_{4,7}, \quad \dot{\rho}_{4,8} = -\gamma\rho_{4,8},$$

$$\dot{\rho}_{5,1} = -i\Omega_{e_1}^*(\rho_{1,1} - \rho_{5,5}) - \gamma\rho_{5,1}, \quad \dot{\rho}_{5,2} = -\gamma\rho_{5,2}, \quad \dot{\rho}_{5,3} = -\gamma\rho_{5,3},$$

$$\dot{\rho}_{5,4} = -\gamma\rho_{5,4}, \quad \dot{\rho}_{5,5} = i\Omega_{e_1}\rho_{5,1} - i\Omega_{e_1}^*\rho_{1,5} - i\Omega_{e_3}\rho_{7,5} + i\Omega_{e_3}^*\rho_{5,7} - \gamma\rho_{5,5},$$

$$\dot{\rho}_{5,6} = -\gamma\rho_{5,6}, \quad \dot{\rho}_{5,7} = i\Omega_{e_3}(\rho_{5,5} - \rho_{7,7}) - \gamma\rho_{5,7}, \quad \dot{\rho}_{5,8} = -\gamma\rho_{5,8},$$

$$\dot{\rho}_{6,1} = -\gamma\rho_{6,1}, \quad \dot{\rho}_{6,2} = -i\Omega_{e_1}^*(\rho_{2,2} - \rho_{6,6}) - \gamma\rho_{6,2},$$

$$\dot{\rho}_{6,3} = -\gamma\rho_{6,3}, \quad \dot{\rho}_{6,4} = -\gamma\rho_{6,4}, \quad \dot{\rho}_{6,5} = -\gamma\rho_{6,5},$$

$$\dot{\rho}_{6,6} = i\Omega_{e_1}\rho_{6,2} - i\Omega_{e_1}^*\rho_{2,6} - \gamma\rho_{6,6}, \quad \dot{\rho}_{6,7} = -\gamma\rho_{6,7}, \quad \dot{\rho}_{6,8} = -\gamma\rho_{6,8},$$

$$\dot{\rho}_{7,1} = -i\Omega_{e_2}^*(\rho_{1,1} - \rho_{7,7}) - \gamma\rho_{7,1}, \quad \dot{\rho}_{7,2} = -\gamma\rho_{7,2}, \quad \dot{\rho}_{7,3} = -\gamma\rho_{7,3},$$

$$\dot{\rho}_{7,4} = -\gamma\rho_{7,4}, \quad \dot{\rho}_{7,5} = -i\Omega_{e_3}^*(\rho_{5,5} - \rho_{7,7}) - \gamma\rho_{7,5}, \quad \dot{\rho}_{7,6} = -\gamma\rho_{7,6},$$

$$\dot{\rho}_{7,7} = i\Omega_{e_2}\rho_{7,1} - i\Omega_{e_1}^*\rho_{1,7} + i\Omega_{e_3}\rho_{7,5} - i\Omega_{e_3}^*\rho_{5,7} - \gamma\rho_{7,7}, \quad \dot{\rho}_{7,8} = -\gamma\rho_{7,8},$$

$$\dot{\rho}_{8,1} = -\gamma\rho_{8,1}, \quad \dot{\rho}_{8,2} = -\gamma\rho_{8,2}, \quad \dot{\rho}_{8,3} = -i\Omega_{e_2}^*(\rho_{3,3} - \rho_{8,8}) - \gamma\rho_{8,3},$$

$$\dot{\rho}_{8,4} = -\gamma\rho_{8,4}, \quad \dot{\rho}_{8,5} = -\gamma\rho_{8,5}, \quad \dot{\rho}_{8,6} = -\gamma\rho_{8,6},$$

$$\dot{\rho}_{8,7} = -\gamma\rho_{8,7}, \quad \dot{\rho}_{8,8} = i\Omega_{e_2}\rho_{8,3} - i\Omega_{e_2}^*\rho_{3,8} - \gamma\rho_{8,8},$$

$$\dot{\rho}_{9,9} = \gamma\rho_{1,1} + \frac{\gamma}{2}(\rho_{5,5} + \rho_{7,7}), \quad \dot{\rho}_{10,10} = \gamma\rho_{2,2} + \frac{\gamma}{2}(\rho_{6,6} + \rho_{7,7}),$$

$$\dot{\rho}_{11,11} = \gamma\rho_{3,3} + \frac{\gamma}{2}(\rho_{5,5} + \rho_{8,8}), \quad \dot{\rho}_{12,12} = \gamma\rho_{4,4} + \frac{\gamma}{2}(\rho_{6,6} + \rho_{8,8}). \quad \text{(B1)}$$

Assuming $\rho_{\ell,\ell'} = \tilde{\rho}_{\ell,\ell'} \exp(-\gamma t)$ $(\ell, \ell' = 1, 2, \ldots, 8)$, we can find that the operator $\tilde{\rho}(t) = \sum_{\ell,\ell'=1}^{8} \tilde{\rho}_{\ell,\ell'} |\Phi_\ell\rangle\langle\Phi'_\ell|$ satisfies the von Neumann equation

$$\dot{\tilde{\rho}}(t) = -i[H_e(t), \tilde{\rho}(t)]. \tag{B2}$$

Consequently, $\tilde{\rho}(t)$ can be calculated by

$$\tilde{\rho}(t) = U_e(t)\rho(0)U_e^\dagger(t), \tag{B3}$$

with $U_e(t)$ being the evolution operator given by the equation $i\dot{U}_e(t) = H_e(t)U_e(t)$. Besides, we define $\rho'(t) = \sum_{\ell=9}^{12} \tilde{\rho}_\ell |\Phi_\ell\rangle\langle\Phi_\ell|$. The matrix elements of $\rho'(t)$ are given by

$$\rho_{9,9}(t) = \frac{\gamma}{2} \int_0^t [2\rho_{1,1}(t') + \rho_{5,5}(t') + \rho_{7,7}(t')]dt',$$

$$\rho_{10,10}(t) = \frac{\gamma}{2} \int_0^t [2\rho_{2,2}(t') + \rho_{6,6}(t') + \rho_{7,7}(t')]dt',$$

$$\rho_{11,11}(t) = \frac{\gamma}{2} \int_0^t [2\rho_{3,3}(t') + \rho_{5,5}(t') + \rho_{8,8}(t')]dt',$$

$$\rho_{12,12}(t) = \frac{\gamma}{2} \int_0^t [2\rho_{4,4}(t') + \rho_{6,6}(t') + \rho_{8,8}(t')]dt'. \tag{B4}$$

Combining the results of Eqs. (B3) and (B4), the density operator $\rho(t)$ can be obtained as Eq. (17).

APPENDIX C: DYNAMIC PHASE AND GEOMETRIC PHASE ACQUIRED IN THE IMPLEMENTATION OF A SINGLE-QUBIT GATE

We now prove that the dynamic (geometric) phase acquired in the time interval $[0, \tau_1]$ is nullified by that acquired in time interval $[\tau_2, T]$. First, we calculate the time derivative of $\beta_2(t)$ in time interval $[\tau_2, T]$ as

$$\frac{d}{dt}\beta_2(t) = \frac{d\tilde{t}}{dt}\frac{d}{d\tilde{t}}[-\Theta_s + \beta_2(\tilde{t})] = -\frac{\tau_1}{T - \tau_2} \times \frac{d}{d\tilde{t}}\beta_2(\tilde{t}), \tag{C1}$$

with $\tilde{t} = \tau_1(T - t)/(T - \tau_2)$. According to Eq. (26), we have

$$\vartheta_-(T) - \vartheta_-(\tau_2) = \int_{\tau_2}^T \frac{\dot{\beta}_2(t)\sin^2[\beta_1(t)]}{2\cos[\beta_1(t)]}dt$$
$$= \int_{\tau_1}^0 \frac{\dot{\beta}_2(\tilde{t})\sin^2[\beta_1(\tilde{t})]}{2\cos[\beta_1(\tilde{t})]}d\tilde{t} = -\vartheta_-(\tau_1),$$

$$\Theta_-(T) - \Theta_-(\tau_2) = -\int_{\tau_2}^T \dot{\beta}_2(t)\sin^2\left[\frac{\beta_1(t)}{2}\right]dt$$
$$= -\int_{\tau_1}^0 \dot{\beta}_2(\tilde{t})\sin^2\left[\frac{\beta_1(\tilde{t})}{2}\right]d\tilde{t} = -\Theta_-(\tau_1). \tag{C2}$$

APPENDIX D: AVERAGE FIDELITY

We now make a brief introduction about the approach to calculate the average fidelity proposed in Ref. [93]. The theorem in Ref. [93] shows that, for any linear operator M on an n-dimensional complex Hilbert space, the uniform average of $|\langle\psi|M|\psi\rangle|^2$ over state vectors $|\psi\rangle$ on the unit sphere S^{2n-1} in $\mathbb{C}^n$ can be calculated by

$$\int_{S^{2n-1}} |\langle\psi|M|\psi\rangle|^2 dV = \frac{1}{n(n+1)}[\text{Tr}(MM^\dagger) + |\text{Tr}(M)|^2], \tag{D1}$$

with dV being the normalized measure on the sphere. First, if M is a Hermitian operator, it can be diagonalized as a diagonal operator Λ by $\Lambda = \mathcal{U}M\mathcal{U}^{-1}$ via a unitary operator $\mathcal{U}$. We denote the left-hand side and right-hand side of Eq. (D1) as $\mathcal{L}(M)$ and $\mathcal{R}(M)$, respectively. By a change of variables $\psi \to \mathcal{U}\psi$, we obtain $\mathcal{L}(\Lambda) = \mathcal{L}(\mathcal{U}M\mathcal{U}^{-1}) = \mathcal{L}(M)$. On the other hand, considering the fact that $\text{Tr}(A_1A_2) = \text{Tr}(A_2A_1)$ for two arbitrary linear operators A_1 and A_2, we obtain $\mathcal{R}(\Lambda) = \mathcal{R}(M)$. Since $\mathcal{L}(\Lambda)$ is a homogeneous polynomial of degree 2 in the real variables $\lambda_1, \lambda_2, \ldots, \lambda_n$, and unitary invariance implies that it is invariant under the exchange of any two λ_J and $\lambda_{J'}$ $(J, J' = 1, 2, \ldots, n)$, consequently the only possible form of $\mathcal{L}(\Lambda)$ is

$$\mathcal{L}(M) = \mathcal{L}(\Lambda) = a_1\text{Tr}(\Lambda^2) + a_2\text{Tr}^2(\Lambda)$$
$$= a_1\text{Tr}(MM^\dagger) + a_2|\text{Tr}(M)|^2, \tag{D2}$$

with a_1 and a_2 being constants related to n. By considering $M_x = |1\rangle\langle2| + |2\rangle\langle1|$, $M_y = -i|1\rangle\langle2| + i|2\rangle\langle1|$, $M_z = |1\rangle\langle1| - |2\rangle\langle2|$, and $M_0 = |1\rangle\langle1| + |2\rangle\langle2|$, we respectively derive

$$\mathcal{L}(M_x) = 2a_1 = 4\int_{S^{2n-1}} \text{Re}(c_1 c_2^*)^2 dV,$$

$$\mathcal{L}(M_y) = 2a_1 = 4\int_{S^{2n-1}} \text{Im}(c_1 c_2^*)^2 dV,$$

$$\mathcal{L}(M_z) = 2a_1 = \int_{S^{2n-1}} (|c_1|^4 + |c_2|^4 - 2|c_1|^2|c_2|^2)dV,$$

$$\mathcal{L}(M_0) = 2a_1 + 4a_2 = \int_{S^{2n-1}} (|c_1|^4 + |c_2|^4 + 2|c_1|^2|c_2|^2)dV, \tag{D3}$$

with $|\psi\rangle = \sum_{J=1}^n c_J|J\rangle$. From Eq. (D3), we obtain $\mathcal{L}(M_x) + \mathcal{L}(M_y) + \mathcal{L}(M_z) = \mathcal{L}(M_0)$, which gives $a_1 = a_2$. Furthermore, by picking the identity operator $\mathbb{1}$ in $\mathcal{L}(\Lambda)$, one can derive $a_1 n + a_2 n^2 = \mathcal{L}(\mathbb{1}) = 1$. Combining the results above, we can derive $a_1 = a_2 = 1/n(n+1)$. Therefore, for a Hermitian operator M, we have $\mathcal{L}(M) = \mathcal{L}(\Lambda) = \mathcal{R}(\Lambda) = \mathcal{R}(M)$.

In fact, the result can also apply to an anti-Hermitian operator A $(A^\dagger = -A)$ since $L(A) = L(iA) = R(iA) = R(A)$. In addition, for a general operator M, it can be decomposed into a Hermitian operator $S = (M + M^\dagger)/2$ and an anti-Hermitian operator $A = (M - M^\dagger)/2$ with $M = S + A$. Accordingly, one can derive

$$\mathcal{L}(S + A) = \mathcal{L}(S) + \mathcal{L}(A) + \int_{S^{2n-1}} \langle\psi|S|\psi\rangle\langle\psi|(A + A^\dagger)|\psi\rangle$$
$$= \mathcal{L}(S) + \mathcal{L}(A),$$

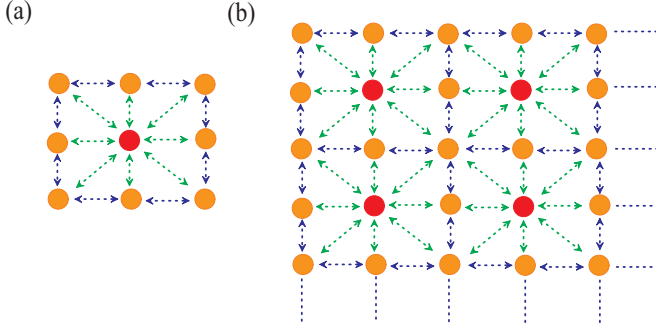(a)   (b)

FIG. 6. (a) Diagrammatic sketch of a possible structure for realizing large-scale quantum computation with a single auxiliary atom. (b) Diagrammatic sketch of a possible structure for realizing large-scale quantum computation with multiple auxiliary atoms in an atom array.

$$\mathcal{R}(S + A) = \frac{1}{n(n+1)}\{\text{Tr}[(S+A)(S-A)]$$
$$+ [\text{Tr}(S) + \text{Tr}(A)][\text{Tr}(S) - \text{Tr}(A)]\}$$
$$= \mathcal{R}(S) + \mathcal{R}(A). \qquad (D4)$$

Using the results of $\mathcal{L}(S) = \mathcal{R}(S)$ and $\mathcal{L}(A) = \mathcal{R}(A)$, we have that the result of Eq. (D1) is satisfied for arbitrary linear operator M. Specially, for quantum gates in a considered $\mathcal{N}$-dimensional computational subspace $\mathcal{S}_c$ (with projection operator $\mathcal{P}_c$), assuming the target operation and real evolution are described by unitary operators $\tilde{U}$ and $U(t)$, the average fidelity over all possible initial states $|\psi\rangle$ in the subspace $\mathcal{S}_c$ should be

$$\bar{F}(t) = \int_{S^{2\mathcal{N}-1}} |\langle\psi|\mathcal{P}_c\tilde{U}^\dagger U(t)\mathcal{P}_c|\psi\rangle|^2 dV, \qquad (D5)$$

with $S^{2\mathcal{N}-1}$ being the unit sphere of the computational subspace $\mathcal{S}_c$. By substituting $M = \mathcal{P}_c\tilde{U}^\dagger U(t)\mathcal{P}_c$, we obtain the formula to calculate the average fidelity used in Eqs. (33) and (45).

APPENDIX E: POSSIBLE EXTENSIONS OF THE PROTOCOL

We now discuss the possible extensions of the protocol to large-scale quantum computation. First, we consider a structure shown in Fig. 6(a), where the red dot in the middle represents an auxiliary atom, and the orange dots around the red dot are the computational atoms. Theoretically, we can realize single-qubit gates for any computational atom with a single auxiliary atom if every atom in this system has strong enough Rydberg interaction strength with the auxiliary atom. In addition, if two adjacent computational atoms have strong enough Rydberg interaction, we can realize two-qubit gates of them with a single auxiliary atom. In the ideal case, the computational atoms remain in their ground states at the beginning and the end of a gate implementation. Therefore, the computational atoms without laser driving would not influence the computational atom being manipulated. Moreover, if the heralded implementation is successful, the auxiliary atom will return to its Rydberg state $|r\rangle$. In this case, the auxiliary atom can continued to be used in the next step of operations. If the measurement result shows that the auxiliary atom is in its ground state $|0\rangle$, the implementation of the quantum gate has failed, and we need to initialize the auxiliary atom to the Rydberg state $|r\rangle$ again. With the structure in Fig. 6(a), it is possible to realize single-qubit gates of all computational atoms and realize two-qubit gates of arbitrary pairs of adjacent atoms. In principle, we may add many computational atoms around the auxiliary atom, but trapping, distant control, and addressing of atoms may become difficult if the number of computational atoms is very large. Therefore, to realize large-scale quantum computation, the atom array shown in Fig. 6(b) may be an alternative candidate. As shown in Fig. 6(b), the atom array is composed of many repeated blocks of atoms shown in Fig. 6(a). The atom in the middle of each block can be used as an auxiliary atom to implement heralded quantum gates. To date, the manipulation of Rydberg atom arrays has been studied in several previous works [100,101], and many interesting results are shown. Therefore, the Rydberg atom array may be a promising platform for large-scale quantum computation.

[1] P. W. Shor, in *1994 Proceedings of the 35th Annual Symposium on Foundations of Computer Science* (IEEE, Washington DC, 1994).

[2] L. K. Grover, Phys. Rev. Lett. **79**, 325 (1997).

[3] G. L. Long, Phys. Rev. A **64**, 022307 (2001).

[4] B. Paredes, F. Verstraete, and J. I. Cirac, Phys. Rev. Lett. **95**, 140501 (2005).

[5] E. Herterich and E. Sjöqvist, Phys. Rev. A **94**, 052310 (2016).

[6] S. L. Zhu and Z. D. Wang, Phys. Rev. Lett. **91**, 187902 (2003).

[7] G. F. Xu, C. L. Liu, P. Z. Zhao, and D. M. Tong, Phys. Rev. A **92**, 052302 (2015).

[8] Z. S. Wang, C. Wu, X. L. Feng, L. C. Kwek, C. H. Lai, C. H. Oh, and V. Vedral, Phys. Rev. A **76**, 044303 (2007).

[9] A. Friedenauer and E. Sjöqvist, Phys. Rev. A **67**, 024303 (2003).

[10] T. Chen and Z. Y. Xue, Phys. Rev. Appl. **10**, 054051 (2018).

[11] E. Sjöqvist, D. M. Tong, L. M. Andersson, B. Hessmo, M. Johansson, and K. Singh, New J. Phys. **14**, 103035 (2012).

[12] G. F. Xu, J. Zhang, D. M. Tong, E. Sjöqvist, and L. C. Kwek, Phys. Rev. Lett. **109**, 170501 (2012).

[13] G. F. Xu, P. Z. Zhao, D. M. Tong, and E. Sjöqvist, Phys. Rev. A **95**, 052349 (2017).

[14] P. Z. Zhao, G. F. Xu, and D. M. Tong, Phys. Rev. A **94**, 062327 (2016).

[15] Z. Y. Xue, J. Zhou, and Z. D. Wang, Phys. Rev. A **92**, 022320 (2015).

[16] Y. H. Kang, Y. H. Chen, Z. C. Shi, B. H. Huang, J. Song, and Y. Xia, Ann. Phys. (Berlin) **531**, 1800427 (2019).

[17] M. V. Berry, Proc. R. Soc. A **392**, 45 (1984).

[18] Y. Aharonov and J. Anandan, Phys. Rev. Lett. **58**, 1593 (1987).

[19] E. Sjöqvist, Physics **1**, 35 (2008).

[20] Q. X. Lv, Z. T. Liang, H. Z. Liu, J. H. Liang, K. Y. Liao, and Y. X. Du, Phys. Rev. A **101**, 022330 (2020).

[21] J. Zhang, T. H. Kyaw, D. M. Tong, E. Sjövist, and L. C. Kwek, Sci. Rep. **5**, 18414 (2015).

[22] S. L. Zhu and P. Zanardi, Phys. Rev. A **72**, 020301(R) (2005).

[23] Z. Zhu, T. Chen, X. Yang, J. Bian, Z. Y. Xue, and X. Peng, Phys. Rev. Appl. **12**, 024024 (2019).

[24] P. Z. Zhao, G. F. Xu, Q. M. Ding, E. Sjöqvist, and D. M. Tong, Phys. Rev. A **95**, 062310 (2017).

[25] I. Fuentes-Guridi, F. Girelli, and E. Livine, Phys. Rev. Lett. **94**, 020503 (2005).

[26] J. Zhang, S. J. Devitt, J. Q. You, and F. Nori, Phys. Rev. A **97**, 022335 (2018).

[27] P. Zanardi and M. Rasetti, Phys. Lett. A **264**, 94 (1999).

[28] L. A. Wu, P. Zanardi, and D. A. Lidar, Phys. Rev. Lett. **95**, 130501 (2005).

[29] L. M. Duan, J. I. Cirac, and P. Zoller, Science **292**, 1695 (2001).

[30] J. Pachos, P. Zanardi, and M. Rasetti, Phys. Rev. A **61**, 010305(R) (1999).

[31] B. J. Liu, X. K. Song, Z. Y. Xue, X. Wang, and M. H. Yung, Phys. Rev. Lett. **123**, 100501 (2019).

[32] S. Li, T. Chen, and Z. Y. Xue, Adv. Quantum Technol. **3**, 2000001 (2020).

[33] Y. H. Kang, Z. C. Shi, B. H. Huang, J. Song, and Y. Xia, Phys. Rev. A **101**, 032322 (2020).

[34] Y. X. Du, Z. T. Liang, H. Yan, and S. L. Zhu, Adv. Quantum Technol. **2**, 1900013 (2019).

[35] N. V. Vitanov, Phys. Rev. A **85**, 032331 (2012).

[36] S. Martínez-Garaot, E. Torrontegui, X. Chen, and J. G. Muga, Phys. Rev. A **89**, 053408 (2014).

[37] Y. C. Li, D. Martínez-Cercós, S. Martínez-Garaot, X. Chen, and J. G. Muga, Phys. Rev. A **97**, 013830 (2018).

[38] Y. H. Kang, Y. H. Chen, Z. C. Shi, B. H. Huang, J. Song, and Y. Xia, Phys. Rev. A **97**, 033407 (2018).

[39] X. Chen, E. Torrontegui, and J. G. Muga, Phys. Rev. A **83**, 062116 (2011).

[40] Y. C. Li, X. Chen, J. G. Muga, and E. Y. Sherman, New J. Phys. **20**, 113029 (2018).

[41] Y. H. Kang, Z. C. Shi, B. H. Huang, J. Song, and Y. Xia, Phys. Rev. A **100**, 012332 (2019).

[42] B. Rousseaux, S. Guerin, and N. V. Vitanov, Phys. Rev. A **87**, 032328 (2013).

[43] D. Ran, W. J. Shan, Z. C. Shi, Z. B. Yang, J. Song, and Y. Xia, Phys. Rev. A **101**, 023822 (2020).

[44] A. Ruschhaupt, X. Chen, D. Alonso, and J. G. Muga, New J. Phys. **14**, 093040 (2012).

[45] X. T. Yu, Q. Zhang, Y. Ban, and X. Chen, Phys. Rev. A **97**, 062317 (2018).

[46] D. Daems, A. Ruschhaupt, D. Sugny, and S. Guérin, Phys. Rev. Lett. **111**, 050404 (2013).

[47] L. Van-Damme, D. Schraft, G. T. Genov, D. Sugny, T. Halfmann, and S. Guérin, Phys. Rev. A **96**, 022309 (2017).

[48] V. A. Mousolou and E. Sjöqvist, Phys. Rev. A **89**, 022117 (2014).

[49] J. Zhang, L. C. Kwek, E. Sjöqvist, D. M. Tong, and P. Zanardi, Phys. Rev. A **89**, 042302 (2014).

[50] G. F. Xu, P. Z. Zhao, T. H. Xing, E. Sjöqvist, and D. M. Tong, Phys. Rev. A **95**, 032311 (2017).

[51] Z. Y. Xue, F. L. Gu, Z. P. Hong, Z. H. Yang, D. W. Zhang, Y. Hu, and J. Q. You, Phys. Rev. Appl. **7**, 054022 (2017).

[52] Z. T. Liang, Y. X. Du, W. Huang, Z. Y. Xue, and H. Yan, Phys. Rev. A **89**, 062312 (2014).

[53] X. K. Song, H. Zhang, Q. Ai, J. Qiu, and F. G. Deng, New J. Phys. **18**, 023001 (2016).

[54] Z. Y. Xue, J. Zhou, Y. M. Chu, and Y. Hu, Phys. Rev. A **94**, 022331 (2016).

[55] B. H. Huang, Y. H. Kang, Z. C. Shi, J. Song, and Y. Xia, Ann. Phys. (Berlin) **530**, 1800179 (2018).

[56] A. A. Abdumalikov, J. M. Fink, K. Juliusson, M. Pechal, S. Berger, A. Wallraff, and S. Filipp, Nature (London) **496**, 482 (2013).

[57] C. Zu, W. B. Wang, L. He, W. G. Zhang, C. Y. Dai, F. Wang, and L. M. Duan, Nature (London) **514**, 72 (2014).

[58] S. Arroyo-Camejo, A. Lazariev, S. W. Hell, and G. Balasubramanian, Nat. Commun. **5**, 4870 (2014).

[59] B. B. Zhou, P. C. Jerger, V. O. Shkolnikov, F. J. Heremans, G. Burkard, and D. D. Awschalom, Phys. Rev. Lett. **119**, 140503 (2017).

[60] Y. Xu, W. Cai, Y. Ma, X. Mu, L. Hu, T. Chen, H. Wang, Y. P. Song, Z. Y. Xue, Z. Q. Yin, and L. Sun, Phys. Rev. Lett. **121**, 110501 (2018).

[61] K. Nagata, K. Kuramitani, Y. Sekiguchi, and H. Kosaka, Nat. Commun. **9**, 3227 (2018).

[62] P. Z. Zhao, X. Wu, T. H. Xing, G. F. Xu, and D. M. Tong, Phys. Rev. A **98**, 032313 (2018).

[63] P. Z. Zhao, G. F. Xu, and D. M. Tong, Phys. Rev. A **99**, 052309 (2019).

[64] Y. H. Kang, Y. H. Chen, Z. C. Shi, B. H. Huang, J. Song, and Y. Xia, Phys. Rev. A **97**, 042336 (2018).

[65] Z. P. Hong, B. J. Liu, J. Q. Cai, X. D. Zhang, Y. Hu, Z. D. Wang, and Z. Y. Xue, Phys. Rev. A **97**, 022332 (2018).

[66] B. J. Liu, Z. H. Huang, Z. Y. Xue, and X. D. Zhang, Phys. Rev. A **95**, 062308 (2017).

[67] D. Shwa, R. D. Cohen, A. Retzker, and N. Katz, Phys. Rev. A **88**, 063844 (2013).

[68] M. Gärttner, Phys. Rev. A **92**, 013629 (2015).

[69] J. E. Johnson, C. Macklin, D. H. Slichter, R. Vijay, E. B. Weingarten, J. Clarke, and I. Siddiqi, Phys. Rev. Lett. **109**, 050506 (2012).

[70] Y. A. Chen, X. H. Bao, Z. S. Yuan, S. Chen, B. Zhao, and J. W. Pan, Phys. Rev. Lett. **104**, 043601 (2010).

[71] J. Borregaard, P. Kómár, E. M. Kessler, A. S. Sørensen, and M. D. Lukin, Phys. Rev. Lett. **114**, 110502 (2015).

[72] W. Qin, X. Wang, A. Miranowicz, Z. Zhong, and F. Nori, Phys. Rev. A **96**, 012315 (2017).

[73] M. M. Müller, M. Murphy, S. Montangero, T. Calarco, P. Grangier, and A. Browaeys, Phys. Rev. A **89**, 032334 (2014).

[74] M. Saffman, J. Phys. B **49**, 202001 (2016).

[75] S. L. Su, E. Liang, S. Zhang, J. J. Wen, L. L. Sun, Z. Jin, and A. D. Zhu, Phys. Rev. A **93**, 012306 (2016).

[76] C. E. Burkhardt, R. L. Corey, W. P. Garver, J. J. Leventhal, M. Allegrini, and L. Moi, Phys. Rev. A **34**, 80 (1986).

[77] D. Vrinceanu, Phys. Rev. A **72**, 022722 (2005).

[78] F. Robicheaux, Phys. Rev. A **56**, R3358(R) (1997).

[79] M. Freitag, J. Heckötter, M. Bayer, and M. Aßmann, Phys. Rev. B **95**, 155204 (2017).

[80] H. R. Lewis and W. B. Riesenfeld, J. Math. Phys. **10**, 1458 (1969).

[81] U. Güngördü, Y. Wan, M. A. Fasihi, and M. Nakahara, Phys. Rev. A **86**, 062312 (2012).

[82] E. Torrontegui, S. Martínez-Garaot, and J. G. Muga, Phys. Rev. A **89**, 043408 (2014).

[83] X. Chen and J. G. Muga, Phys. Rev. A **86**, 033405 (2012).

[84] R. S. Kaushal and H. J. Korsch, J. Math. Phys. **22**, 1904 (1981).

[85] S. Ahmad and A. Ambrosetti, *A Textbook on Ordinary Differential Equations*, La Matematica per il 3+2, Vol. 88 (Springer, Cham, 2015).

[86] By applying pulses with contrary-sign detunings, we can offset the Stark-shifts of ground states. For example, considering $\tilde{H}_1(t)$ in Eq. (A3), the Stark shifts caused by the pulses with blue detunings are described by $H_{ss1}(t) = \frac{|\Omega_1(t)|^2}{\Delta_1}(|0++\rangle_{012}\langle 0++| + |0+-\rangle_{012}\langle 0+-| - |0r+\rangle_{012}\langle 0r+| - |0r-\rangle_{012}\langle 0r-|) + \frac{|\Omega_2(t)|^2}{\Delta_1}(|0++\rangle_{012}\langle 0++| + |0-+\rangle_{012}\langle 0-+| - |0+r\rangle_{012}\langle 0+r| - |0-r\rangle_{012}\langle 0-r|)$. Stark shifts caused by the pulses with red detunings can be described by $-H_{ss1}(t)$. Thus, the total Stark shifts on ground states $|0\pm\pm\rangle_{0,1,2}$ are offset. By calculating the Stark shifts with $\tilde{H}_2(t)$ and $\tilde{H}_3(t)$ in Eq. (A3), we can obtain similar results.

[87] Here, the Rydberg interaction strengths are considered to be the same for the simplicity of discussions. In fact, the Rydberg interaction strengths between each pair of atoms can be different. We can see from Eq. (A3) that terms with oscillation frequencies in the scale of V are omitted. Therefore, when the Rydberg interaction strengths become different, as long as they are much larger compared with detunings and Rabi frequencies of laser pulses, we can obtain the same result as Eq. (A3).

[88] S. L. Su, Y. Tian, H. Z. Shen, H. Zang, E. Liang, and S. Zhang, Phys. Rev. A **96**, 042335 (2017).

[89] X. Q. Shao, D. X. Li, Y. Q. Ji, J. H. Wu, and X. X. Yi, Phys. Rev. A **96**, 012328 (2017).

[90] L. N. Ji, T. Chen, and Z. Y. Xue, Phys. Rev. A **100**, 062312 (2019).

[91] Z. T. Liang, X. Yue, Q. Lv, Y. X. Du, W. Huang, H. Yan, and S. L. Zhu, Phys. Rev. A **93**, 040305(R) (2016).

[92] P. Zanardi and D. A. Lidar, Phys. Rev. A **70**, 012315 (2004).

[93] L. H. Pedersen, N. M. Møller, and K. Mølmer, Phys. Lett. A **367**, 47 (2007).

[94] T. Wilk, A. Gaëtan, C. Evellin, J. Wolters, Y. Miroshnychenko, P. Grangier, and A. Browaeys, Phys. Rev. Lett. **104**, 010502 (2010).

[95] D. X. Li and X. Q. Shao, Phys. Rev. A **98**, 062338 (2018).

[96] R. H. Zheng, Y. H. Kang, D. Ran, Z. C. Shi, and Y. Xia, Phys. Rev. A **101**, 012345 (2020).

[97] Y. M. Liu, X. D. Tian, D. Yan, Y. Zhang, C. L. Cui, and J. H. Wu, Phys. Rev. A **91**, 043802 (2015).

[98] K. Singer, J. Stanojevic, M. Weidemüller, and R. Côté, J. Phys. B: Atom. Mol. Opt. Phys. **38**, S295 (2005).

[99] D. F. V. James and J. Jerke, Can. J. Phys. **85**, 625 (2007).

[100] R. Samajdar, W. W. Ho, H. Pichler, M. D. Lukin, and S. Sachdev, Phys. Rev. Lett. **124**, 103601 (2020).

[101] C. J. Lin, V. Calvera, and T. H. Hsieh, Phys. Rev. B **101**, 220304(R) (2020).